

Process mining-driven modeling and simulation to enhance fault diagnosis in cyber-physical systems

Francesco Vitale^a, Nicola Dall’Ora^{b,c}, Sebastiano Gaiardelli^b, Enrico Fraccaroli^b, Nicola Mazzocca^a, Franco Fummi^b

^a*University of Naples Federico II, Department of Electrical Engineering and Information Technology, Via Claudio, 21, Naples, 80125, Italy*

^b*University of Verona, Department of Engineering for Innovation Medicine*

(Section of Engineering and Physics), Strada le Grazie, 15, Verona, 37134, Italy

^c*Guglielmo Marconi University, Department of Engineering Sciences, Via Plinio, 44, Rome, 00193, Italy*

Abstract

Cyber-Physical Systems (CPSs) tightly interconnect digital and physical operations within production environments, enabling real-time monitoring, control, optimization, and autonomous decision-making that directly enhance manufacturing processes and productivity. The inherent complexity of these systems can lead to faults that require robust and interpretable diagnoses to maintain system dependability and operational efficiency. However, manual modeling of faulty behaviors requires extensive domain expertise and cannot leverage the low-level sensor data of the CPS. Furthermore, although powerful, deep learning-based techniques produce black-box diagnostics that lack interpretability, limiting their practical adoption. To address these challenges, we set forth a method that performs unsupervised characterization of system states and state transitions from low-level sensor data, uses several process mining techniques to model faults through interpretable stochastic Petri nets, simulates such Petri nets for a comprehensive understanding of system behavior under faulty conditions, and performs Petri net-based fault diagnosis. The method begins with detecting collective anomalies involving multiple samples in low-level sensor data. These anomalies are then transformed into structured event logs, enabling the data-driven discovery of interpretable Petri nets through process mining. By enhancing these Petri nets with timing distributions, the approach supports the simulation of faulty behaviors. Finally, faults can be diagnosed online by checking collective anomalies with the Petri nets and the corresponding simulations. The method is applied to the Robotic Arm Dataset (RoAD), a benchmark collected from a robotic arm deployed in a scale-replica smart manufacturing assembly line. The application to RoAD demonstrates the method’s effectiveness in modeling, simulating, and classifying faulty behaviors in CPSs. The modeling results demonstrate that our method achieves a satisfactory interpretability-simulation accuracy trade-off with up to 0.676 arc-degree simplicity, 0.395 R^2 , and 0.088 RMSE. In addition, the fault identification results show that the method achieves an F1 score of up to 98.925%, while maintaining a low conformance checking time of 0.020 seconds, which competes with other deep learning-based methods.

Keywords: Fault diagnosis, Simulation, Modeling, Classification, Process mining.

1. Introduction

The integration of physical and cyber processes in modern Cyber-Physical Systems (CPSs) offers significant opportunities to enhance service quality in the manufacturing sector, enabling real-time monitoring, control, optimization, and autonomous decision-making, and ensuring a range of characteristics, such as flexibility, scalability, and adaptability [1]. However, the resulting complexity of CPSs calls for adequate means to ensure system reliability despite the presence of vulnerabilities and occurrence of run-time faults [2]. Therefore, achieving high reliability involves the prompt detection of anomalies, accurately determining their root causes, and proactively planning recovery actions [3]. In addition, simulation frameworks have become indispensable tools to support the development of reliable production systems, accelerate CPS development, perform what-if analyses, and design effective recovery strategies [4, 5].

Although many studies have explored anomaly detection in CPSs, these approaches are mostly limited to characterizing

normal behavior and identifying deviations from it. However, anomalies do not automatically translate into faults, which are defined as “adjudged or hypothesized causes” of an error [6]. To analyze and identify faults, we adopt a broader perspective from recent literature [7, 8, 9], in which diagnosis extends beyond anomaly detection to include identifying and classifying root causes. Within this view, modeling and simulation become essential tools for examining how faults arise and propagate, as well as for planning corrective actions. Accordingly, our work intends to provide structure and insight to support fault diagnosis rather than limiting itself to anomaly detection.

Despite the high demand for interpretable and comprehensive fault diagnosis methods, most approaches still focus on capturing normal patterns in historical sensor data and flag anomalous trends, which, as said, do not provide further information about the type of anomaly that occurred and cannot provide an insightful root cause analysis [10]. Besides, these approaches are often based on advanced deep learning methods,

which, although powerful and extremely accurate, have limited interpretability [11]. On the other hand, other formalisms can be employed to model and simulate faulty behaviors, including Petri nets, widely accepted due to their clear, process-based semantics. These aspects, especially, facilitate interpretability, a quality increasingly critical in trustworthy artificial intelligence applications [12, 13, 14, 15]. Yet, existing interpretable Petri net-based approaches either require manual, error-prone modeling by domain experts [16, 17, 18, 19] or do not directly target data-driven modeling of faulty CPS behaviors from low-level sensor data, requiring domain knowledge to supervise the capture of normal behavior into a Petri net and discriminate such behavior from anomalies [20, 21, 22]. Hence, a notable gap persists regarding the data-driven modeling of faulty CPS behaviors through Petri nets directly from low-level sensor data, particularly within frameworks that offer both predictive power and explanatory transparency.

To provide interpretable detection, simulation, and classification of faulty CPS behavior, we investigate process mining, whose algorithms allow data-driven discovery of Petri nets (process discovery), enhancements of such Petri nets with a time perspective (process enhancement), and comparing new behavior with the Petri nets to evaluate their alignment (conformance checking) [12]. Specifically, we propose a process mining-driven method for fault diagnosis that begins with isolating anomalous CPS behaviors through collective anomaly detection, which allows identifying anomalous behaviors involving multiple sensor data samples. Then, such data is converted into structured event logs unsupervisedly through clustering. The event logs are used to extract interpretable Petri nets through process discovery and to enrich them with actual timings from the collected data via process enhancement. These Petri nets enable detailed stochastic simulations, providing more insights into system behavior and supporting robust fault classification. Finally, conformance checking between online data, the stochastic Petri nets, and their corresponding simulations is performed for fault diagnosis.

In summary, the novelty of our method involves:

- Unsupervised characterization of manufacturing CPS states, state transitions, state times, and state times distribution from low-level sensor data;
- Integration of process mining to build interpretable Petri nets based on the control-flow relations of state transitions, enhanced with the time perspective of the state times distributions;
- Simulating the stochastic Petri nets to have a comprehensive understanding of the states traversed by the system and their timings under faulty conditions;
- Petri net-based fault diagnosis by isolating anomalous behavior and checking its alignment to the faults characterized offline, allowing the interpretable identification of different fault types.

We demonstrate our method’s capabilities in modeling accuracy, simulation fidelity, and fault diagnosis effectiveness

in smart manufacturing, referencing the Robotic Arm Dataset (RoAD), a benchmark collected from a robotic arm deployed in a scale-replica smart manufacturing assembly line. The modeling results demonstrate that our method achieves a satisfactory interpretability-simulation accuracy trade-off with up to 0.676 arc-degree simplicity, 0.395 R^2 and 0.088 RMSE. In addition, the fault identification results show that the method achieves an F1 score of up to 98.925%, while maintaining a low conformance checking time of 0.020 seconds, which competes with other deep learning-based methods.

The remainder of the article is structured as follows: Section 2 reviews relevant literature on process mining and Petri nets, positioning our contributions and novelty clearly within the existing state-of-the-art. Section 3 details the proposed process mining-driven method for fault diagnosis. Section 4 empirically assesses the methodology’s effectiveness using the RoAD benchmark. Finally, Section 5 summarizes key insights and outlines potential future research directions.

2. Background

Fault diagnosis in CPSs is intrinsically difficult. Hybrid continuous/discrete dynamics, large-scale multivariate sensor streams, and the stringent demand for interpretable decisions in safety-critical domains collectively pose technical and methodological challenges. Classical solutions ranging from first-principles physical models and fuzzy rule bases to neural network-driven classifiers have proven effective in specific settings; yet they typically (i) require extensive domain expertise, (ii) offer limited transparency, and (iii) provide little support for realistic behavioral simulation [11].

To address these limitations, we propose a process mining-driven fault diagnosis method that effectively integrates data-driven learning with the formal structure of Petri nets, whose synergy with data-centric approaches has been demonstrated in prior works [23, 24, 25]. Unlike black-box models, process mining generates explicit, executable representations of system behavior. The remainder of this section introduces the necessary preliminaries on process mining and Petri nets, then surveys existing CPS fault-diagnosis research to position our contribution.

2.1. Preliminaries

Process mining comprises two core activities: *process discovery* and *conformance checking* [12]. Process discovery builds a process model (here, a Petri net) from historical event logs, whereas conformance checking quantifies how closely new logs align with a reference Petri net. An event log is a collection of *cases*; each case records a time-ordered sequence of *events* corresponding to state transitions in the underlying CPS.

Definition 2.1 (Event, trace, case, event log). *Let \mathcal{E} be the universe of events, \mathcal{ST} the universe of state transitions, and \mathcal{T} the universe of timestamps. Given $e \in \mathcal{E}$, denote its state transition and timestamp by $\#_{st}(e) \in \mathcal{ST}$ and $\#(e) \in \mathcal{T}$, respectively. A trace is an ordered sequence $\sigma = \langle e_1, \dots, e_k \rangle$ with $e_i \in \mathcal{E}$; the set of all*

traces is \mathcal{E}^* . Let C denote the universe of cases and $\#_{\text{trace}}(c) \in \mathcal{E}^*$ the trace associated with case $c \in C$. An event log is a finite subset $L \subseteq C$.

In this study, we focus on the control-flow relations and timing distributions extracted from event logs and captured via labeled accepting Petri nets.

Definition 2.2 (Labeled accepting Petri net). *Let P and Tr be disjoint node sets ($P \cap Tr = \emptyset$) in a bipartite graph, and let $F \subseteq (P \times Tr) \cup (Tr \times P)$ be the set of directed arcs. A Petri net is the triple (P, Tr, F) . Its marking $M \in \mathcal{B}(P)$ is a multiset of tokens and encodes the current state. Petri nets that have an initial marking M_0 and a final marking M_f , i.e., an initial and final state, are called accepting Petri nets. Furthermore, consider a set of state transitions $ST \subseteq \mathcal{ST}$ and a labeling function $l_{Tr} : Tr \rightarrow ST \cup \{\tau\}$, where τ denotes a silent (unobservable) transition. A labeled accepting Petri net is the tuple $(P, Tr, F, M_0, M_f, ST, l_{Tr})$. N denotes the universe of all labeled accepting Petri nets, hereafter referred to as Petri nets.*

The formal semantics of Petri nets include the ability to fire a transition. Given the number of incoming arcs of a transition, if the current marking is such that there is at least a token in each place connected to the transition, it can fire, i.e., the transition consumes one token from each incoming place and generates one token for each outgoing arc. This firing dynamic enables the Petri net to evolve its state, allowing for the above-mentioned conformance checking and simulation. In addition, it is worth noting that there is a special class of Petri nets, namely workflow Petri nets, which have two specific places: a source place and a sink place. In these Petri nets, M_0 assigns a token to the source place. Any complete firing sequence moves the Petri net state from M_0 to M_f , which consists of at least a token in the sink place. Notably, a desirable property of Petri nets is the *soundness*. A Petri net is sound if any firing sequence from the initial marking can reach a unique final marking without leaving dead transitions [12].

When each transition of a Petri net is further annotated with a firing rate, the model becomes a *stochastic Petri net* [26].

Definition 2.3 (Stochastic Petri net). *Given a Petri net $N = (P, Tr, F, M_0, M_f, ST, l_{Tr}) \in \mathcal{N}$, let \mathcal{D} be a set of probability distributions and $\delta : Tr \rightarrow \mathcal{D}$ assign each transition $tr \in Tr$ its firing-time distribution d_{tr} . The triple $N_s = (N, \delta, \mathcal{D})$ is termed a stochastic Petri net.*

Figure 1 shows an illustrative workflow stochastic Petri net. In particular, the left part shows the control-flow view of the Petri net, consisting of transitions tr_1, \dots, tr_6 , two silent (τ) transitions, the source and sink places, and intermediate places. The control-flow structure constrains the allowable traces of the Petri net, which can be simulated with the firing logic described above. For example, trace $\langle tr_1, tr_2, tr_3, tr_4, tr_5, tr_2, tr_6 \rangle$ can be simulated since it is a legal firing sequence. The process is as follows. tr_1 fires, producing tokens that enable tr_2 , tr_3 , and tr_4 . tr_2 and tr_3 partially enable tr_6 , while tr_4 enables tr_5 , which also partially enables tr_6 . After τ fires, tr_2 can fire again, further enabling tr_6 . Finally, tr_6 fires, using tokens from tr_2 , tr_3 , and tr_5 ,

to produce the final token and complete the process. Clearly, when more transitions are concurrently enabled, the simulation engine must resolve race conditions [27].

In addition to the control-flow structure, the time perspective, shown on the right part, allows integrating a time duration into the simulations. For example, the firing-time distribution d_{tr_1} is such that the time associated with tr_1 firing may last either 0 to 10 seconds with 49.2% probability, 10 to 20 seconds with 40.2% probability, 20 to 30 seconds with 10.0% probability, 30 to 40 seconds with 0.4% probability, or 40 to 50 seconds with 0.2% probability. The enhancement of the control-flow structure with the time perspective allows reducing the gap between the Petri net and the actual CPS dynamics.

2.2. Related works

To further contextualize our contribution, we revisit traditional model-based techniques, followed by hybrid approaches that attempt to incorporate data-driven insights into Petri net-based fault diagnosis.

2.2.1. Model-based approaches

Early research on fault diagnosis in industrial systems proposed Petri nets as a reasoning tool to understand the root causes of system-wide failures [16]. Subsequently, research aimed to synchronize the fault-free and faulty behaviors within the same Petri net, enabling controllers to identify faults and enforce recovery actions to ensure system safety. For example, Liu et al. [17] modeled the fault-error-failure chain of a home CPS using a stochastic Petri net, pairing model elements with the layered view of the system. Furthermore, Nazemzadeh et al. [18] proposed a method to integrate faults in fault-free Petri nets. They defined fault models as tuples of Petri net elements, including faulty transitions that, when activated, lead to errors. The diagnosability of faults on Petri nets depends on whether the observed behavior provides sufficient information to identify the activation of faulty transitions. To check if observed behavior causes the activation of faulty transitions, a diagnoser (a model-checking routine) determines the activation of faulty transitions. Several proposals have introduced different diagnosers based on assumptions about the reference Petri net (e.g., transition types and labeling) and the model-checking routine used (e.g., integer linear programming) [28, 29, 30].

2.2.2. Hybrid approaches

Modeling Petri nets for complex CPSs is challenging and error-prone [19]. Consequently, researchers have begun to leverage data-driven insights to integrate faulty behavior into fault-free Petri nets. For example, Zhu et al. [31] formulated a set of integer linear programming constraints to incorporate faulty behavior into fault-free Petri nets and identify the root causes of faults. Similarly, Hou et al. [32] proposed an alternative data-driven method to discover faulty Petri nets. This method utilizes transition incidence matrices obtained from system traces to address the NP-hard nature of integer linear programming approaches.

More recently, process mining has been applied to fault diagnosis and simulation. Neshastegaran et al. [33] developed a

Table 1: Comparative summary of research on Petri net-based hybrid fault diagnosis, classified according to data type, research area, fault diagnosis method, and simulation support.

Reference	Data type	Research area	Simulation	Fault diagnosis method
[31]	High-level event data	Integer linear programming	No	Data-driven extension of a fault-free Petri net to include faulty transitions
[32]	High-level event data	Transition incidence matrices	No	Data-driven extension of a fault-free Petri net to include faulty transitions
[33]	High-level event data	Process discovery	No	Data-driven modeling of the overall behavior of an industrial system with the Petri net to reason about the root causes of faulty behavior
[34]	High-level event data	Process discovery	No	Data-driven modeling of the normal behavior of an industrial system with the Petri net and ad-hoc introduction of faulty behavior into the model
[35]	High-level event data	Process discovery Conformance checking	No	Data-driven modeling of the normal behavior of information systems with the Petri net and verification of deviations from the model of run-time data
[20]	Low-level sensor data	Process discovery Conformance checking	No	Data-driven modeling of the normal behavior of an industrial system with the Petri net and verification of deviations from the model of run-time data
[36]	Low-level sensor data	Process discovery	No	Data-driven modeling of the normal behavior of an industrial system with the Petri net and verification of deviations from the model of run-time data
[37]	High-level event data	Conformance checking	Yes	Verification of deviations from the Petri net of run-time data
[21]	High-level event data	Process discovery Conformance checking Process enhancement	No	Data-driven modeling of the overall behavior of an industrial system with the Petri net to reason about the root causes of faulty behavior
[22]	Low-level sensor data	Process discovery Conformance checking	Yes	Data-driven modeling of the normal behavior of an industrial system with the Petri net and verification of deviations from the model of run-time data
Our work	Low-level sensor data	Process discovery Conformance checking Process enhancement	Yes	Data-driven modeling of the faulty behavior of an industrial system with the Petri net to reason about the root causes of faulty behavior

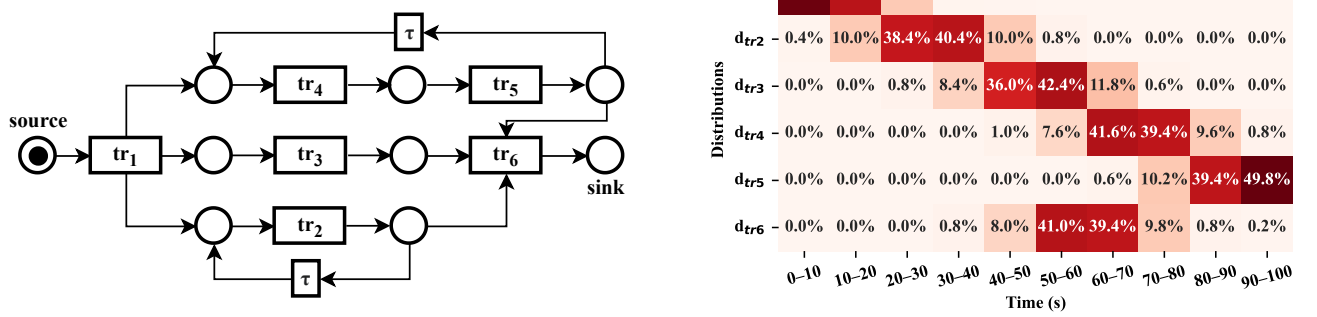


Figure 1: Illustrative workflow stochastic Petri net. The left figure shows the control-flow structure, while the right figure depicts the time perspective.

topology of an industrial plant through process discovery, leveraging monitored events to enhance the understanding of potential faults. Friederich et al. [34] proposed a process mining-based framework for reliability modeling of smart manufacturing processes. The framework integrates the fault-free Petri net obtained through process discovery with custom fault models for each manufacturing resource. Wang et al. [35] propose a method that combines neural network-based anomaly detection with process mining. Their method first involves modeling normal behavior using a Petri net from discrete logs collected, for example, from network data and software executions. Next, they perform neural network-based anomaly detection to identify anomalous traces in run-time event logs. Finally, the anomalous traces are checked against the normal behavior to analyze the deviations and provide an explanation of the deviating behavior. Vitale et al. [20] and Shi et al. [36] proposed using process discovery and conformance checking to characterize normal behavior from low-level sensor data of industrial systems through Petri nets and check deviations from such behavior. They proposed various unsupervised techniques to discretize sensor data, enabling the use of process discovery and conformance checking. De Benedictis et al. [37] used conformance checking to evaluate whether digital twins could detect new runtime faults. These faults arise from faulty simulations generated from a Petri net of a proof-of-concept Industrial Internet of Things application. Beyel et al. [21] introduced a method of connecting high-level event data from a CPS in the automotive domain with Petri nets developed through process discovery. They demonstrated how this method enables the analysis of time spent in CPS states and the frequency of the transitions between them over time. Vitale et al. [22] provided an unsupervised approach to characterizing the state transitions of an industrial CPS involving a real water distribution testbed case study. Their approach involved characterizing the normal CPS behavior through process discovery and checking any deviations from it through conformance checking.

2.2.3. Novelty of our work

Table 1 characterizes the reviewed hybrid approaches according to the data type used, the approach followed, the fault diagnosis method, and whether Petri net-based simulations were performed.

Data type. Many prior works mostly dealt with high-level event data annotated with the specific activity being carried out in the target industrial system. While labeled data allows for the seamless connection of actual events with the system under observation, its availability is limited in real-world applications. Unlike these works, our proposal deals with *low-level sensor data* and extracts states and state transitions unsupervisedly.

Research area. Earlier approaches primarily extended manually designed fault-free Petri nets by integrating faulty transitions with normal behavior. More recent works have shifted toward Petri net-based fault diagnosis through process discovery, conformance checking, or a combination of both. Our work aligns with this emerging direction by integrating discovery, conformance checking, and process enhancement in a unified method.

Simulation. Petri net-based simulation for industrial systems has only been explored by a few of the works we reviewed. Additionally, the simulations performed in these works focus solely on control flow, attempting to replicate the sequences of activities and/or state transitions captured in the Petri net. On the other hand, we aim to integrate the time perspective into our simulations by mining stochastic Petri nets with time distributions for each state transition, thereby allowing for a faithful replication of the actual system's behaviors.

Fault diagnosis method. Petri net-based fault diagnosis using process mining has largely focused on modeling the normal or overall behavior of a system and then verifying deviations from that model. Such approaches essentially reduce to anomaly detection. In contrast, our method directly captures faulty behaviors and encodes them in specific Petri nets, enabling both fault identification and root-cause analysis. This shift—from detecting deviations to isolating and classifying faults through interpretable Petri nets—distinguishes our approach from earlier work.

Contextualization. We contextualize our proposal within the Monitor-Analyze-Plan-Execute over a shared Knowledge (MAPE-K) architecture (see Figure 2), a well-established framework for autonomous systems [38]. Our method especially enhances the *Analyze* phase through event log extraction,

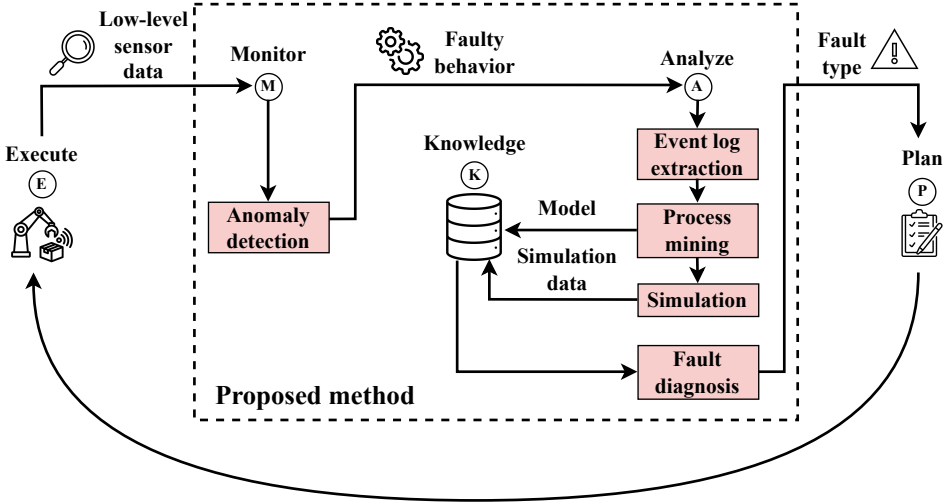


Figure 2: The MAPE-K architecture in which our proposed method is contextualized. The red boxes indicate the different phases of our method.

process mining, simulation, and fault diagnosis, linking offline root-cause analysis with online fault diagnosis. This integration can significantly improve informed decision-making and facilitate proactive corrective actions in manufacturing systems.

3. Method

This section describes the proposed process mining-driven method for fault diagnosis. The method is split into an offline part and an online part. The offline part is organized into four phases, aiming to capture different fault types into stochastic Petri nets. These are used in the online fault diagnosis phase, which performs fault diagnosis by comparing anomalous behavior with both the structure of the stochastic Petri nets and their offline-generated simulations. The five phases are illustrated in Figure 3 and are detailed in the following sections.

3.1. Phase 1: Anomaly detection

The objective of this phase is to isolate anomalous behavior from normal behavior in manufacturing CPSs. Notably, these systems collect large amounts of low-level sensor data in the form of multivariate time series, which can include anomalies [39]. As a result, this phase specifically involves detecting anomalous behavior from these data.

Definition 3.1 (Multivariate time series). *Let us denote $\mathcal{T} = \{t_i : i \in \{0, \dots, o-1\}, o \in \mathbb{N}\}$ a set of timesteps up to $o \in \mathbb{N}$. A multivariate time series ts with p features is defined as follows.*

$$ts = \{(t_i, ts(t_i)) : t_i \in \mathcal{T}, x(t_i) \in \mathbb{R}^p\}. \quad (1)$$

In the following, we refer to a multivariate time series of o samples and p features as $ts \in \mathbb{R}^{o \times p}$.

Multivariate time series anomaly detection has become highly effective, especially due to advancements in deep learning approaches that can accurately discriminate normal patterns

from anomalous ones [40, 41, 42, 43]. While these approaches have achieved excellent results, they are unable to characterize and classify faults, as their objective is to model normal patterns and flag anomalous observations. Phase 1 builds on these abilities and isolates collective anomalies in time series, defined as sequences of contiguous samples that deviate from expected patterns [44, 45]. We refer to such sequences as **anomalous time series windows**.

Definition 3.2 (Anomalous time series window). *Let $ts \in \mathbb{R}^{o \times p}$ be a multivariate time series with p features and o samples. Let $ts(i) \in \mathbb{R}^p$ be a time series sample at timestep $t_i \in \mathcal{T}$. Let $t_k, t_l \in \mathcal{T}, k < l \leq o$. A time series window $ts_{k,l}$ is the set:*

$$ts_{k,l} = \{ts(t_j) \in \mathbb{R}^p : t_j \in \mathcal{T}, t_k \leq t_j \leq t_l\} \subseteq ts. \quad (2)$$

In the following, we refer to an anomalous time series window of anomaly A as $W_A \subseteq ts$ and denote $\mathcal{W}_A = \{W_{A,1}, W_{A,2}, \dots, W_{A,\psi}\}$ the set of ψ anomalous time series windows of anomaly A isolated from ts .

The sets $\mathcal{W}_{A_1}, \mathcal{W}_{A_2}, \dots, \mathcal{W}_{A_m}$ capture m different fault types. Figure 3 demonstrates this concept by decomposing a historical time series ts into multiple time series windows, where a normal pattern is disrupted by anomalies A_1 and A_2 . These are isolated and collected into sets \mathcal{W}_{A_1} and \mathcal{W}_{A_2} , which are passed on to the next step for event log extraction.

3.2. Phase 2: Event log extraction

The objective of this phase is the processing of low-level sensor data and their conversion into event logs so that process mining algorithms can be applied. To this aim, the phase first involves characterizing data as sequences of events. Common approaches for discretizing time series data and extracting event logs involve grouping each sample into clusters [46, 20, 47] or by identifying specific events, such as increasing or decreasing trends and specific activities [48, 36, 22]. While the latter

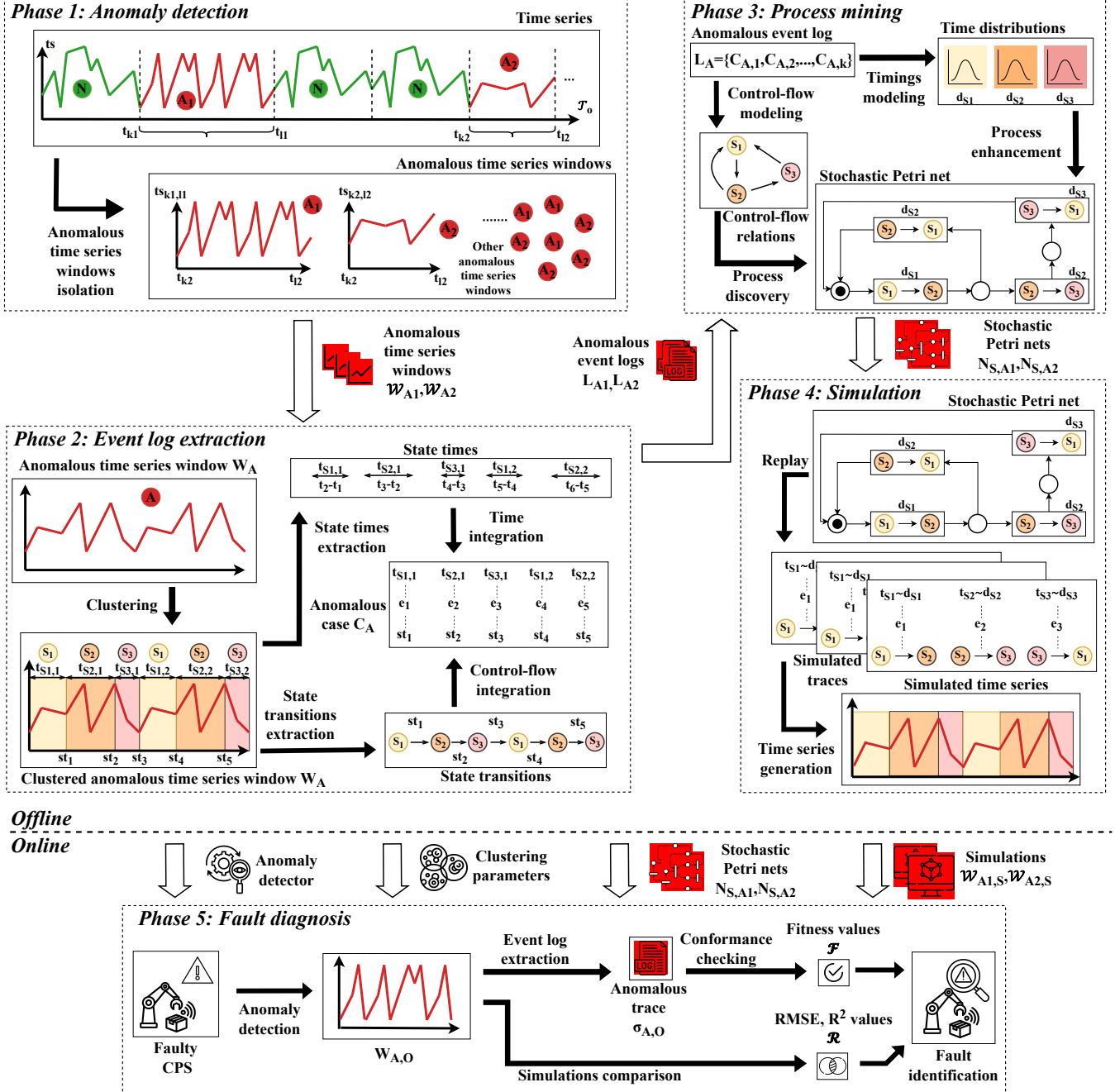


Figure 3: The process mining-driven method for fault diagnosis, organized into an offline part and an online part. The offline part involves four phases, which aim to 1) isolate anomalous time series windows; 2) extract state transitions and state times unsupervisedly; 3) mine stochastic Petri nets characterizing faulty behavior; and 4) simulate the Petri nets to analyze the faulty behavior and support fault identification. Online fault diagnosis uses the outputs of the four phases to isolate and identify CPS faults.

approaches are more precise in identifying events from sensor data, they require domain knowledge and, in some cases, accurate labeling. On the other hand, clustering-based approaches are unsupervised and very valuable in contexts where the collected data is not labeled or the manual identification of possible trends is impractical. Hence, our proposal adopts the first class of methods and clusters time series values into a set of **states** and collects events by identifying transitions between clusters, i.e., the **state transitions**.

Definition 3.3 (State and state transition). *Let $W_A \subseteq ts \in \mathbb{R}^{o \times p}$ be an anomalous time series window isolated from a and $\mathcal{S} = \{s_1, \dots, s_\alpha : s_i \in \mathbb{R}^p, \alpha \in \mathbb{N}\}$ be a set of clusters obtained by assigning W_A values to α centroids. We define $s_t \in \mathcal{S}, t \in \mathcal{T}_o$ the state associated with $ts(t) \in W_A$. Therefore, \mathcal{S} is the set of states. Given $t_k, t_l : 0 \leq k < l \leq o$, there is a state transition associated with t_l if $\forall t_j : t_k < t_j < t_l, s_{t_j} = s_{t_k}$ and $s_{t_k} \neq s_{t_l}$. An event e associated with the pair of states s_{t_k}, s_{t_l} is such that $\#_{st}(e) = s_{t_l} = s_{t_k} \rightarrow s_{t_l}$ and $\#_t(e) = t_l$. The state s_{t_k} is associated with s_{t_l} .*

The application of this definition requires extracting the set of states \mathcal{S} by applying a suitable clustering algorithm to the original time series ts from which the anomalous time series windows are isolated. Numerous such algorithms are documented in the literature. Arguably, an increasing number of clusters leads to a more complex state space with a possibly better discretization of the time series.

Figure 3 shows how a given anomalous time series window W_A gets discretized through clustering into an alternation of three different states, namely s_1 , s_2 , and s_3 . Each state s has a given duration t_s that depends on the time instant at which a state transition occurs. To integrate the time perspective into the Petri nets, the **state times** are collected.

Definition 3.4 (State time). *Let \mathcal{S} be a set of states, $e \in \mathcal{E}$ be an event, and $\#_{st}(e) = s_{t_k} \rightarrow s_{t_l}$ a state transition. The state time of $s_{t_k} \in \mathcal{S}$ associated with $\#_{st}(e)$ is $t_l - t_k$.*

Each anomalous time series window W_A corresponds to an anomalous case C_A . C_A collects the sequence of state transitions in W_A and the associated state times. The set of cases collected from set W_A composes the anomalous event log L_A . In conclusion, the anomalous event logs L_{A_1} and L_{A_2} of anomalies A_1 and A_2 are passed on to phase 3.

3.3. Phase 3: Process mining

The objective of this phase is to encode the anomalous event logs into stochastic Petri nets to build a fault dictionary. To this aim, the anomalous event log L_A of a given anomaly A is processed in two different ways through process discovery and process enhancement.

3.3.1. Process discovery

To discover the control-flow structure, the relations between the different state transitions within the cases of L_A are captured. For example, by analyzing all the cases of L_A , it may result that states s_1 and s_2 repeat in a loop, state s_3 always follows

s_2 , and s_1 always follows s_3 . Process discovery can encode these control-flow relations into a Petri net, which ultimately represents the CPS behavior under faulty conditions.

Definition 3.5 (Process discovery algorithm). *Let $L \subseteq C$ be an anomalous event log. A process discovery algorithm is a function γ that captures the control-flow relations among the state transitions of the cases of L and encodes them to a Petri net $N \in \mathcal{N}$: $\gamma(L) = N$.*

The set of control-flow relations discovered by γ depends on the specific process discovery algorithm being used. For example, the inductive miner [49] identifies several types of control-flow relations, such as sequence, parallel, exclusive, and redo-loop relations. It does this by splitting the event log into simpler segments, which enables the recognition of these relations. The integer linear programming-based miner [50] finds causal relations between the activities of an event log and specifies a system of inequalities to find the so-called regions, i.e., two sets of activities such that the prior execution of the first set enables the execution of the second set. The heuristics miner [51] finds dependency relations between the activities of an event log through the dependency graph, which collects frequency-based causal relations between activities based on their occurrences in the event log.

Notably, the inductive miner, integer linear programming-based miner, and heuristics miner discover workflow Petri nets. However, the types of control-flow relations identified by the process discovery algorithm determine the range of possible Petri nets the algorithm can generate. This constraint is known as the *representational bias*, and can significantly impact the quality of the resulting Petri net [12]. In turn, this could impact the ability to adequately characterize the faulty behavior.

The aforementioned biases may cause two different phenomena in the resulting Petri nets: overfitting and underfitting. For example, although the inductive miner builds perfectly fitting Petri nets from the data, it forces this property by introducing many silent transitions. This results in the Petri net being underfit, i.e., it introduces many more behaviors than those present in the observed data. Yet, while the integer linear programming-based miner limits the introduction of silent transitions, it enforces many constraints in building the above-mentioned regions through the system of inequalities, thereby leading to overfitting Petri nets; i.e., the model is very specific to the data at hand. Finally, the heuristics miner may also lead to overfitting Petri nets by attempting to capture all the causal relations, including the infrequent ones. To mitigate the underfitting and overfitting phenomena, the algorithms were extended with filtering mechanisms that allow reducing the impact on the resulting Petri net [12].

In our study, we are particularly interested in reducing the overfitting effect while maintaining a good degree of specificity, i.e., avoiding underfitting. By attempting to model the behavior of complex and noisy event logs, the resulting Petri net may have numerous places and arcs, resulting in an overwhelming structure whose interpretation can be cumbersome and challenging. To quantitatively evaluate the interpretability of the Petri net, the arc-degree simplicity can be used [52].

Definition 3.6 (Arc-degree simplicity). Let $N \in \mathcal{N}$ be a Petri net and $arc_{P,N}, arc_{Tr,N} \in \mathbb{N}$ the total number of incoming and outgoing arcs in N related to, respectively, the set P of places and the set Tr of transitions. Let $arc_N \in arc_{P,N} \cup arc_{Tr,N}$ be the arc degree of N . The arc-degree simplicity S_{arc} of N is:

$$S_{arc}(N) = \frac{1}{1 + (\overline{arc} - 2)}, \overline{arc} = \frac{1}{|arc_N|} \sum_{x \in arc_N} x. \quad (3)$$

According to the arc-degree simplicity, the simplest Petri net ($S_{arc} = 1$) has exactly one incoming and one outgoing arc per node. The more complex the dynamics, the more incoming and outgoing arcs per node there are, the closer to 0 S_{arc} becomes, and the less interpretable the Petri net is.

3.3.2. Process enhancement

Once a quality Petri net is built with process discovery, process enhancement is performed to integrate the time perspective into the Petri net [12]. Such enhancement involves collecting the **state time distributions** from the cases of the anomalous event log.

Definition 3.7 (State time distribution). Let L_A be the anomalous event log associated with anomaly A and $s \in \mathcal{S}$ a state. Let $T_s = \{t_{s,e} \in \mathbb{R} : \#_{st}(e) = s \rightarrow \bar{s}, e \in L_A\}$ be the set of state times associated with s found in the events of the cases of L_A . The state time distribution $d_s : \mathbb{R} \rightarrow \mathbb{R}$ is a function that models the probability based on T_s that s lasts for a certain time.

The integration of the state time distributions in the Petri net, as illustrated in Section 2, allows adding the time perspective. In the case of Figure 3, the three states have time distributions d_{s_1} , d_{s_2} , and d_{s_3} assigned to each of the four transitions. The resulting enhanced model constitutes a **stochastic Petri net** that supports simulation and quantitative analysis of the temporal behavior of the process. By combining process discovery with temporal enhancement, the model provides a more realistic and analytically powerful representation of the faulty CPS, enabling both diagnosis and predictive evaluation of anomalous system dynamics. In conclusion, the stochastic Petri nets N_{S,A_1} and N_{S,A_2} of anomalies A_1 and A_2 are passed on to phase 4.

3.4. Phase 4: Simulation

The objective of this phase involves simulating the Petri net to analyze the faulty behavior and provide synthetic yet realistic anomalous time series windows.

First, the simulation **replays** a stochastic Petri net to generate new traces. A simulated trace is of the form $\langle st_1, \dots, st_f \rangle$. A state is associated with each state transition of the trace. E.g., if $st_1 = s \rightarrow \bar{s}$, with s_β and s_γ being two states of the CPS, then s is associated with st_1 . At each state in the simulated trace, a corresponding state time is randomly selected from the state time distribution linked with that transition. As a result, the sequence of state transitions is transformed into state-state time pairs. The sequence of state-state time pairs is the **simulated time series window**.

Definition 3.8 (Simulated time series window). Let $N \in \mathcal{N}$ be a Petri net, $\mathcal{S} = \{s_1, \dots, s_\alpha : s_i \in \mathbb{R}^p, \alpha \in \mathbb{N}\}$ a set of α states, $\mathcal{D} = \{d_1, \dots, d_\alpha : d_i : \mathbb{R} \rightarrow \mathbb{R}, \alpha \in \mathbb{N}\}$ the set of state time distributions, δ the function that associates the state time distributions with the state transitions of N , and $N_S = (N, \delta, \mathcal{D})$ a stochastic Petri net. Let $\sigma_{sim} = \langle st_1, \dots, st_k \rangle$ be a trace of k state transitions obtained by replaying N_S . The corresponding simulated time series window is the sequence of pairs $\langle (s_{st_1}, t_{st_1}), \dots, (s_{st_k}, t_{st_k}) \rangle$. The i -th pair (s_{st_i}, t_{st_i}) captures the state $s_{st_i} \in \mathcal{S}$ associated with st_i and the corresponding state time t_{st_i} sampled from \mathcal{D} .

It is worth mentioning that, as explained in Section 2, the generated traces — and their conversion into time series windows using the approach above — depend on both the control-flow structure and the time perspective. While the control-flow structure may fit the faulty behavior, the set of allowable traces can be broader than those actually seen in the data, as the process discovery algorithms attempt to capture as much structure as possible. Likewise, the state time distributions are random variables that probabilistically sample a time to associate with states. Hence, the resulting traces capture the stochastic essence of the anomalous process, striking a balance between model generality and realistic temporal variability.

3.5. Phase 5: Fault diagnosis

The online part of the method involves performing fault diagnosis using the outputs provided by the offline phases, namely the anomaly detector trained during phase 1, the clustering parameters of phase 2, the stochastic Petri nets of phase 3, and the simulations of phase 4.

The faulty CPS is monitored and the anomaly detector used to isolate the anomalous time series window $W_{A,O}$ from the normal behavior. Next, after the anomalous trace $\sigma_{A,O}$ is obtained by applying event log extraction using the same clustering parameters as those obtained during phase 2, the fault is diagnosed by combining two different approaches: **conformance checking** and **simulations comparison**.

Conformance checking involves evaluating the degree of similarity between a trace and the structure of the stochastic Petri net. There are various algorithms for performing such checks. The state-of-the-art conformance checking algorithm is the alignment-based one [12]. This approach attempts to find the best path across the reference stochastic Petri net that most accurately approximates the traces in the event log that deviate from normal control flow. This is achieved by considering the log moves in an event log and their alignment with the reference stochastic Petri net, as determined by evaluating the corresponding model moves. This alignment is compared to the worst-case alignment, and the fitness is calculated using a cost function η that quantifies the alignment's penalty for each misaligned pair of log and model moves.

Definition 3.9 (Fitness). Let $\sigma_{A,O}$ be the anomalous trace and N a Petri net. Moreover, let $\gamma_N^*(\sigma_{A,O})$ and $\gamma_N^w(\sigma_{A,O})$ be the optimal and worst alignments of $\sigma_{A,O} \in L$ with respect to N , respectively. Finally, let $\eta(\gamma_N^*(\sigma_{A,O}))$ and $\eta(\gamma_N^w(\sigma_{A,O}))$ be the costs

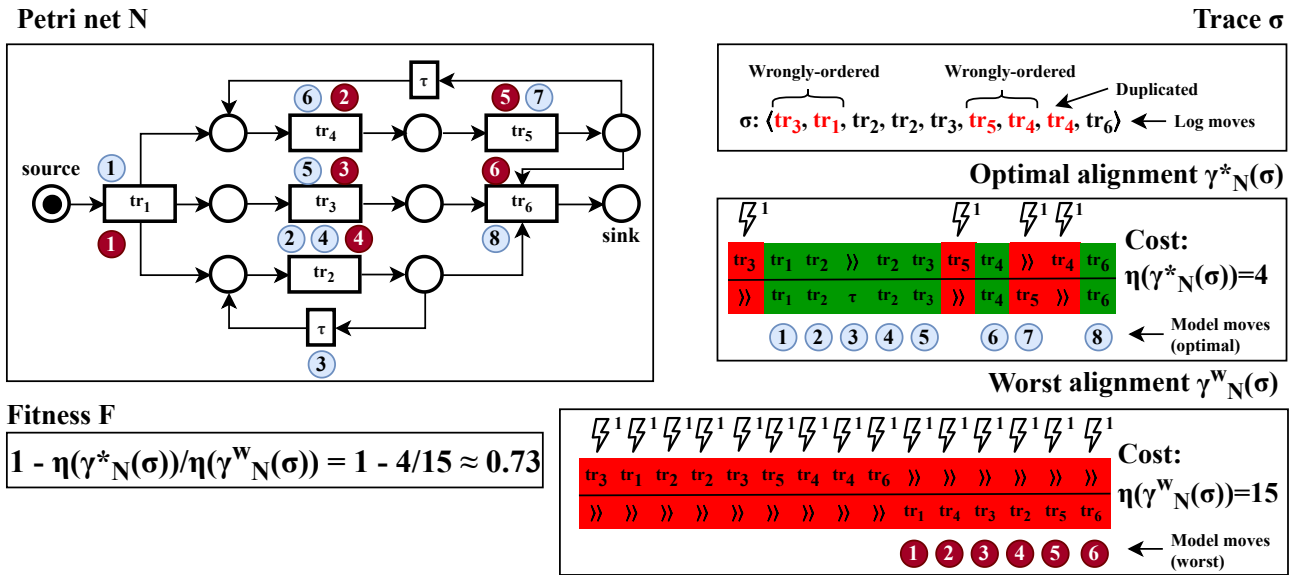


Figure 4: Example fitness calculation between a trace σ and the control-flow structure of Petri net N of Figure 1.

assigned to the optimal and worst alignments, respectively. The fitness $F_{\sigma_{A,O}} \in [0, 1]$ is

$$F(\sigma_{A,O}, N) = 1 - \frac{\eta(\gamma_N^*(\sigma_{A,O}))}{\eta(\gamma_N^w(\sigma_{A,O}))}. \quad (4)$$

Figure 4 shows an example fitness calculation based on the optimal and worst alignment of an example trace $\sigma = \langle tr_3, tr_1, tr_2, tr_2, tr_3, tr_5, tr_4, tr_4, tr_6 \rangle$ with respect to the control-flow structure of the Petri net N shown in Figure 1. The trace has several control-flow anomalies, including wrongly-ordered and duplicated transitions. When finding the optimal alignment $\gamma_N^*(\sigma)$, these anomalies translate into “unsynchronized” moves, i.e., there is no possible matching between the log and model moves of the alignment. By considering the worst alignment as the shortest firing sequence on the model following all the log moves, the costs of the best and worst alignments sum to, respectively, 4 and 15, leading to a fitness $F(\sigma, N)$ of approximately 0.73.

Simulations comparison involves evaluating the difference between the anomalous time series window and the simulations performed offline. Several metrics can be used for this purpose. In our method, we consider two metrics: the Root Mean Squared Error (RMSE) and the coefficient of determination (R^2):

$$\text{RMSE} = \sqrt{\frac{1}{n} \sum_{i=1}^n (W_{A,O}(i) - W_{A,S}(i))^2}, \quad (5)$$

$$R^2 = 1 - \frac{\sum_{i=1}^n (W_{A,O}(i) - W_{A,S}(i))^2}{\sum_{i=1}^n (W_{A,O}(i) - \bar{W}_{A,O})^2}, \quad (6)$$

where $W_{A,S}$ is a simulated window and n is the number of samples of the windows. While RMSE evaluates the similarity of the simulation to the amplitude of the actual signal, R^2 provides information about the difference in explained variance between the actual signal and the simulated window.

The fault identification part of fault diagnosis uses these three metrics according to Algorithm 1. The algorithm identifies the best candidates for each of the three metrics and makes a final decision based on the majority among them.

Algorithm 1 Fault identification

```

1: Input:  $N_{S,A_1}, \dots, N_{S,A_m}, W_{A_1,S}, \dots, W_{A_m,S}, W_{A,O}, \sigma_{A,O}$ 
2: Output: Fault type
3:  $\mathcal{F}, \mathcal{R}_{\text{RMSE}}, \mathcal{R}_{\text{R}^2} \leftarrow \{\}, \{\}, \{\}$ 
4: for  $i = 1$  to  $m$  do
5:    $\mathcal{F}, \mathcal{R}_{\text{RMSE}}, \mathcal{R}_{\text{R}^2} \leftarrow \mathcal{F} \cup \{\mathcal{F}(\sigma_{A,O}, N_{S,A_i})\}, \mathcal{R}_{\text{RMSE}} \cup \{\text{RMSE}(W_{A,O}, W_{A_i,S})\}, \mathcal{R}_{\text{R}^2} \cup \{\text{R}^2(W_{A,O}, W_{A_i,S})\}$ 
6: end for
7: Indices  $\leftarrow (\arg \max \mathcal{F}, \arg \min \mathcal{R}_{\text{RMSE}}, \arg \max \mathcal{R}_{\text{R}^2})$ 
8: Fault type  $\leftarrow \text{majority}(\text{Indices})$ 
9: return Fault type

```

4. Case study

We apply the process mining-driven fault diagnosis method to the Robotic Arm Dataset (RoAD) case study [53], whose dataset is one of the best representatives in the manufacturing CPS context, as reported in the work of Golendukhina et al. [54] and Khan et al. [55]. The goals of the experiments involve analyzing:

- The impact of key methodology factors on the unsupervised modeling and simulation quality of faulty CPS behaviors (modeling and simulation quality).
- The ability to identify different faulty CPS behaviors and clearly distinguish them from one another to build a fault dictionary (fault identification).

We evaluate the effectiveness of the methodology in modeling and simulating faulty time series windows collected from the RoAD dataset. The discussion below describes the RoAD case study and the application of the method to it, providing an overview of the experiments and a detailed discussion of the results, which outline the findings and potential threats to the validity of the experimentation.

4.1. RoAD dataset

4.1.1. Physical Plant

The RoAD case study comprises real multivariate time series data collected from various sensors mounted on a Kuka robotic arm, a collaborative robotic arm deployed in a scaled replica of a manufacturing process, as shown in the top-right corner of Figure 5. The robotic arm is integrated into a fully-fledged production line located in the Industrial Computer Engineering (ICE) Laboratory¹, a cutting-edge research facility at the University of Verona dedicated to cyber-physical production systems. This production line includes a diverse set of industrial-grade machines, representative of modern smart manufacturing environments: a quality control cell with high-resolution laser scanners and cameras for visual inspection, a robotic assembly cell with two collaborative robotic manipulators for flexible handling tasks, a subtractive manufacturing cell equipped with a four-axis computer numerical control milling machine, and a functional control cell that integrates a flying probe system for automated functional testing. Two automated guided vehicles manage the internal logistics, transporting goods between the warehouse and the conveyor belt, enabling the emulation of complex material flows. The KUKA robotic arm plays a pivotal role within this system, performing critical operations such as assembly, disassembly, and tightening. The production line is based on the flexible manufacturing paradigm. Rather than adhering to rigid, predefined workflows, it enables the dynamic composition of manufacturing processes by orchestrating a set of reusable processing capabilities offered by each work cell. This configuration not only mirrors the adaptability required in

Industry 4.0 scenarios but also provides a high-fidelity experimental environment for evaluating advanced automation, orchestration strategies, and verification techniques under realistic conditions.

4.1.2. Sensor data

At the top-left corner of Figure 5 is a schematic of the physical plant and the set of sensors, labeled 0 to 6, deployed across its structure. The multivariate time series of each sensor includes measurements from accelerometers, gyroscopes, and power consumption sensors. The recorded multivariate time series reflects both nominal and anomalous behaviors of the KUKA robotic arm. The identified anomalies are categorized into distinct classes. In this study, we focus on the X, Y, and Z axis accelerations recorded by sensor 2, as they clearly capture both regular and anomalous behaviors. At the bottom of Figure 5, three acceleration time series sampled at 10 Hz are shown: ts_N , ts_V , and ts_W . The normal time series, ts_N , alternates between two recurring patterns, N_1 and N_2 , at regular intervals of approximately 50 samples (5 seconds). These two patterns correspond to distinct activities within the manufacturing workflow: picking up an object and moving it to another location. To simulate anomalies, two modified time series were collected: ts_V and ts_W , corresponding to velocity and weight anomalies, respectively. The velocity anomaly reduces the robot's movement speed, affecting pattern N_1 . This alteration, annotated as A_V , manifests as slower dynamics and lower acceleration amplitudes. Conversely, the weight anomaly increases the object's mass, affecting pattern N_2 . This alteration, annotated as A_W , is characterized by slower motion and a distinctive step-like acceleration pattern.

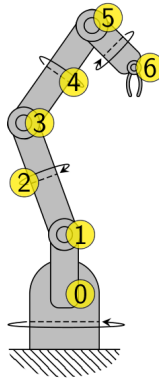
Method application. We aim to capture the faulty CPS behavior through our methodology as follows. First, we set out a controlled environment for the experiments by manually tuning the anomaly detection step to fixed accuracy configurations. This allows us to evaluate the impact of the anomaly detection part on the subsequent fault diagnosis phase. Next, we apply the event log extraction and process mining steps to either of the weight and velocity time series windows to obtain stochastic Petri nets capturing the faulty CPS behavior. Furthermore, we simulate the reference Petri net a given number of times and evaluate the alignment of the simulated time series windows with the original faulty CPS behavior. Finally, we evaluate the effectiveness of our proposal in identifying different types of faults.

4.1.3. Experimental setup

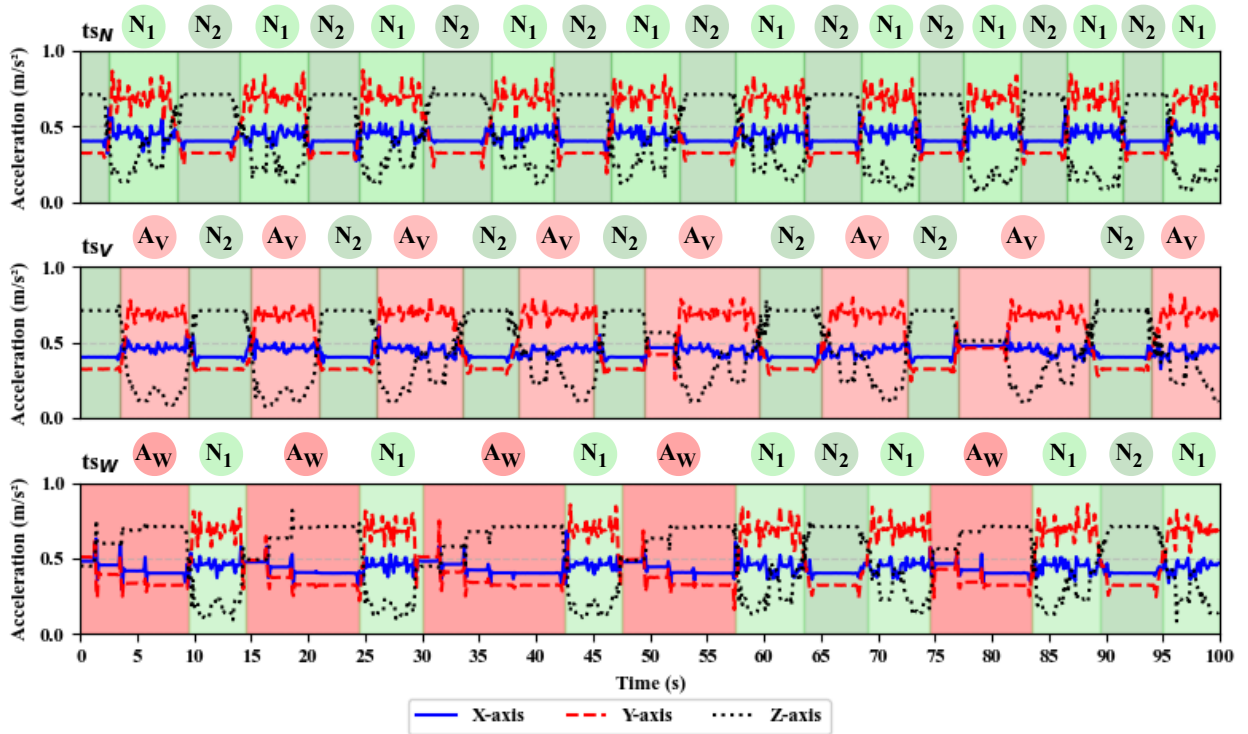
Hardware and Software Specifications. The software for the experiments was implemented using Python and run on a Windows 10 machine with an Intel Core i9-11900K CPU at 3.50 GHz and 32GB of RAM. The software uses machine learning and PM libraries, such as `scikit-learn` and `pm4py`. In addition, it includes a set of DOS batch scripts to automatically replicate the experiments carried out in this work, publicly

¹<https://www.icelab.di.univr.it/laboratory>

KUKA robotic arm



ICE lab's smart manufacturing line



Sensor ② X, Y and Z axis acceleration of the KUKA robotic arm

Figure 5: Experimental setup of the Robotic Arm Dataset (RoAD) testbed at the ICE laboratory of the University of Verona. The smart manufacturing line integrates a KUKA robotic arm instrumented with seven sensors at each mechanical joint, measuring the X, Y, and Z-axis acceleration. The sensor 2 acceleration values are captured in three different conditions: normal (ts_N), weight anomaly (ts_W), and velocity anomaly (ts_V). Each time series either show the normal patterns N_1 and N_2 or anomalous patterns AV and AW .

available on GitHub².

Data pre-processing and simulation. The sensor data was pre-processed so that controlled experimentation could be carried out. The resulting dataset properties after pre-processing are shown in Table 2. First, ts_N , ts_V and ts_W were normalized between 0 and 1. Second, 10000 samples for each time series of

²https://github.com/francescovitale/pm_based_modeling_simulation.

Table 2: The RoAD dataset properties.

Property	ts _N	ts _V	ts _W
Samples	10000 (\approx 16 min.)		
Features	3 (X, Y and Z acc.)		
Windows	161	159	76
Window size	49	62	130
Normal windows	161	79	37
Anomalous windows \mathcal{W}_A	0	80	48
Training windows $\mathcal{W}_{A,tr}$	0	48	23
Test windows $\mathcal{W}_{A,tst}$	0	32	16

sensor 2 of the robotic arm were retrieved. Third, we manually extracted time series windows to obtain a labeled dataset with which we evaluate the method’s performance. Specifically: ts_N has a total of 161 normal windows, with an average window size of 49 samples; ts_V has a total of 159 windows, of which 79 are normal and 80 are anomalous, with an average window size of 62 samples; ts_W has a total of 130 windows, of which 37 are normal and 48 are anomalous, with an average window size of 130 samples. We split each set of anomalous windows \mathcal{W}_A into a training set $\mathcal{W}_{A,tr}$ and a test set $\mathcal{W}_{A,tst}$, using a simple 75% holdout procedure. Finally, during the simulation, we set the number of traces to simulate to 300 and, for each trace, generate the simulated time series according to Definition 3.8. The number of simulated time series windows was sufficient to extract a statistically reliable estimation of how different the simulated Petri net was compared to the actual time series windows. We repeat this procedure three times to obtain mean and standard deviation statistics for the metrics used to evaluate the modeling and simulation quality and fault identification capabilities.

4.1.4. Factors

The key factors influencing the method’s capabilities involve the anomaly detection accuracy, the clustering algorithm, and the process discovery algorithm. The accuracy of anomaly detection depends on the number of true positives (TP), false positives (FP), true negatives (TN), and false negatives (FN). Positives are anomalous time series windows, whereas negatives are normal time series windows. Therefore, anomaly detection accuracy:

$$Acc = \frac{TP + TN}{TP + TN + FP + FN} \quad (7)$$

is changed by varying the content of the training windows $\mathcal{W}_{A,tr}$. For example, if the accuracy is perfect, the set only contains true positives. If the accuracy is 75%, 25% of true positives are replaced with the same percentage of false positives. The clustering algorithm employed in the experiments to extract the state, state transitions, and state time from the time series is K-means, a well-known clustering technique that associates each data point with a single cluster. This technique is desirable as it allows the user to specify the desired number of clusters to be extracted. The K factor relates to the number of states and state transitions that can be captured. For example, if K equals 3, the CPS dynamics are discretized into 3 states

and 6 state transitions. Hence, the higher K, the finer-grained the discretization is. The process discovery techniques used to extract the Petri net from the anomalous event log are the Inductive Miner Infrequent (IMf) [56], Integer Linear Programming-based Miner (ILP) [50], and Heuristics Miner (HM) [51]. These three techniques can tolerate noise in event logs and utilize three distinct approaches to discover control-flow relations, which allows evaluating the representational bias impact outlined in Section 3. To minimize the impact of noise in event logs while minimizing excessive filtering, we set the noise threshold for these three algorithms to 75%.

4.1.5. Metrics

The metrics used in the first experiment to evaluate the Petri net quality are the arc-degree simplicity (Equation 3), RMSE (Equation 5), and R² (Equation 6). The second experiment to evaluate the fault identification capabilities involves the F1-score (F1), calculated as follows. Let $\mathcal{W}_{A,target}$ be the anomalous time series windows of the target fault to identify. These are the positive samples. Furthermore, let $\mathcal{W}_{A,other}$ be the anomalous time series windows of the other fault. These are the negative samples. F1 is:

$$F1 = \frac{2TP}{2TP + FP + FN}. \quad (8)$$

Furthermore, to assess the online capabilities of our method, we include the conformance checking time, which is the time needed to perform alignment-based conformance checking for a single trace.

4.2. Modeling and simulation quality

To assess the impact of clustering and process discovery configurations on modeling and simulation metrics, we outline a two-factor full factorial experiment, where the first factor is K, and the second factor is the process discovery algorithm. Table 3 reports the method results for the S_{arc}, R² and RMSE metrics. Additionally, Figure 6 shows the S_{arc}, R², and RMSE trends for each process discovery algorithm with an increasing number of clusters K.

4.2.1. Results

S_{arc} impact. The interpretability of the Petri net in terms of S_{arc} tends to drop for each process discovery algorithm as K increases. This trend is especially true for the ILP, for which S_{arc} drops abruptly starting from K=3 for both the velocity and weight anomalies. This trend is true for the IMf and HM too, although it tends to stabilize for both anomalies (S_{arc} \geq 0.552). Such low S_{arc} values for the ILP are due to its tendency to produce overfitting Petri nets, as the algorithm attempts to compact too many behaviors in the same control-flow structure. In turn, the ILP appears unsuitable for low-level sensor data due to the very low interpretability of its resulting Petri nets.

R² impact. The impact on R² is especially evident for low K values, for which the simple state space is unable to capture the variability of the low-level sensor data. For example, considering the HM and weight anomaly for K=2, R² is equal to

Table 3: The modeling and simulation quality results of the offline part of our fault diagnosis method for both the velocity and weight anomaly. Bold numbers highlight the best R^2 per process discovery algorithm and anomaly type. The grey cells highlight the best Petri nets for the velocity and weight anomalies in terms of simplicity (S_{arc}), coefficient of determination (R^2), and RMSE trade-off.

ILP (75% noise tolerance)				IMf (75% noise tolerance)			HM (75% noise tolerance)			
K	S_{arc}	R^2	RMSE	S_{arc}	R^2	RMSE	S_{arc}	R^2	RMSE	
Velocity anomaly	2	0.666 _{0.000}	-0.235 _{0.319}	0.135 _{0.073}	0.742 _{0.005}	-0.198 _{0.147}	0.110 _{0.059}	1.000 _{0.000}	-11.524 _{15.702}	0.218 _{0.105}
	3	0.210 _{0.063}	0.073 _{0.040}	0.087 _{0.012}	0.772 _{0.032}	0.087 _{0.026}	0.081 _{0.006}	0.649 _{0.012}	0.032 _{0.019}	0.101 _{0.009}
	4	0.109 _{0.005}	0.173 _{0.073}	0.074 _{0.006}	0.701 _{0.009}	0.203 _{0.024}	0.079 _{0.003}	0.607 _{0.005}	0.078 _{0.061}	0.101 _{0.015}
	5	0.064 _{0.011}	0.187 _{0.101}	0.076 _{0.006}	0.673 _{0.024}	0.345 _{0.066}	0.067 _{0.003}	0.595 _{0.008}	0.209 _{0.082}	0.082 _{0.016}
	6	0.038 _{0.006}	0.052 _{0.040}	0.078 _{0.005}	0.628 _{0.005}	0.229 _{0.057}	0.060 _{0.016}	0.567 _{0.004}	0.126 _{0.034}	0.067 _{0.000}
	7	0.037 _{0.001}	0.242 _{0.029}	0.059 _{0.007}	0.597 _{0.013}	0.024 _{0.242}	0.068 _{0.027}	0.564 _{0.004}	0.182 _{0.120}	0.076 _{0.012}
	8	0.024 _{0.004}	0.345 _{0.054}	0.065 _{0.006}	0.585 _{0.022}	0.126 _{0.223}	0.093 _{0.028}	0.563 _{0.003}	0.252 _{0.084}	0.066 _{0.007}
	9	0.032 _{0.003}	0.157 _{0.108}	0.100 _{0.006}	0.619 _{0.019}	-0.376 _{0.788}	0.111 _{0.036}	0.552 _{0.004}	-0.213 _{0.257}	0.121 _{0.055}
	10	0.024 _{0.004}	0.233 _{0.065}	0.067 _{0.005}	0.592 _{0.021}	-1.090 _{0.888}	0.226 _{0.075}	0.569 _{0.001}	-0.343 _{0.154}	0.213 _{0.065}
	11	0.032 _{0.003}	0.267 _{0.114}	0.082 _{0.016}	0.587 _{0.011}	-4.903 _{7.114}	0.116 _{0.052}	0.566 _{0.004}	-0.135 _{0.245}	0.133 _{0.076}
	12	0.018 _{0.002}	0.233 _{0.065}	0.069 _{0.008}	0.589 _{0.012}	-7.192 _{7.829}	0.217 _{0.026}	0.573 _{0.002}	-0.270 _{0.065}	0.158 _{0.046}
Weight anomaly	2	0.600 _{0.000}	-0.260 _{0.248}	0.137 _{0.023}	0.750 _{0.000}	-0.126 _{0.298}	0.128 _{0.028}	1.000 _{0.000}	-25.046 _{1.777}	0.394 _{0.036}
	3	0.219 _{0.006}	-0.321 _{0.151}	0.148 _{0.022}	0.689 _{0.017}	-0.153 _{0.188}	0.138 _{0.014}	0.641 _{0.007}	-0.488 _{0.126}	0.161 _{0.039}
	4	0.095 _{0.005}	0.144 _{0.126}	0.092 _{0.010}	0.683 _{0.016}	0.305 _{0.049}	0.092 _{0.008}	0.636 _{0.009}	0.196 _{0.059}	0.087 _{0.016}
	5	0.064 _{0.005}	0.296 _{0.068}	0.077 _{0.005}	0.721 _{0.012}	0.284 _{0.014}	0.092 _{0.007}	0.642 _{0.005}	-1.564 _{2.523}	0.224 _{0.162}
	6	0.064 _{0.003}	0.268 _{0.019}	0.087 _{0.005}	0.676 _{0.019}	0.395 _{0.072}	0.088 _{0.008}	0.634 _{0.018}	-0.866 _{1.435}	0.217 _{0.153}
	7	0.030 _{0.001}	0.337 _{0.086}	0.078 _{0.005}	0.631 _{0.008}	0.314 _{0.095}	0.101 _{0.020}	0.592 _{0.008}	-1.901 _{2.963}	0.207 _{0.173}
	8	0.045 _{0.004}	0.219 _{0.073}	0.083 _{0.004}	0.669 _{0.015}	0.296 _{0.079}	0.092 _{0.004}	0.616 _{0.005}	0.242 _{0.067}	0.090 _{0.001}
	9	0.037 _{0.004}	0.277 _{0.072}	0.070 _{0.009}	0.658 _{0.011}	0.296 _{0.079}	0.070 _{0.004}	0.654 _{0.009}	-1.803 _{2.457}	0.257 _{0.146}
	10	0.038 _{0.007}	0.312 _{0.064}	0.069 _{0.007}	0.674 _{0.015}	0.358 _{0.100}	0.084 _{0.011}	0.659 _{0.019}	-0.944 _{1.696}	0.203 _{0.161}
	11	0.017 _{0.001}	0.210 _{0.024}	0.096 _{0.003}	0.663 _{0.012}	0.124 _{0.022}	0.100 _{0.009}	0.641 _{0.012}	-2.743 _{2.283}	0.320 _{0.144}
	12	0.029 _{0.006}	0.171 _{0.062}	0.100 _{0.009}	0.664 _{0.010}	0.142 _{0.031}	0.090 _{0.009}	0.647 _{0.007}	-2.800 _{0.425}	0.415 _{0.016}

-25.046, which indicates a strong lack of variance explanation by the simulated version of the signal. This is also true for the ILP and IMf, which reveal low R^2 values for $K=2$ (-0.235 and -0.198 for the velocity anomaly and -0.260 and -0.126 for the weight anomaly). However, R^2 tends to increase for all the process discovery algorithms. For example, the IMf peaks, for the velocity anomaly and weight anomaly, at 0.345 for $K=5$ and 0.395 for $K=6$, respectively. However, as the state space increases in complexity, R^2 tends to drop. This is true for all process discovery algorithms, although the ILP appears to be more stable. Still, the IMf achieves the highest R^2 for both anomaly types (0.345 for $K=5$ and 0.395 for $K=6$).

RMSE impact. RMSE values follow a trend very similar to R^2 , although less visible due to the metric being concerned with amplitudes rather than variance. However, it is quite clear, especially from the IMf and HM, that the RMSE achieves a minimum value and then begins to rise again. For example, the RMSE of the IMf, for the velocity and weight anomaly, drops down to 0.060 for $K=6$ and 0.088 for $K=6$, and then rises up to 0.226 for $K=10$ and 0.100 for $K=11$. Again, the ILP appears to be more stable than the other two; however, the IMf is the most balanced, which confirms that it achieves the best trade-off among the three metrics.

4.2.2. Interpretation and root cause analysis

The Petri nets built by the process discovery algorithms can be linked to the physical properties of the CPS thanks to the characterization of the state transitions (Definition 3.3) and

state time distributions (Definition 3.7) of our method. Figure 7 shows the control-flow structure and time perspective of the velocity (top) and weight (bottom) Petri nets built by the IMf with $K=5$. The velocity windows at the top and weight windows at the bottom have been clustered into regions (the colored segments in the windows' plots) in the event log extraction phase of the method. Each cluster s represents a triple (x, y, z) , where the three elements are the centroid values of the robotic arm's acceleration at the selected joint. Therefore, each state transition can be linked to CPS dynamics, and replicated through the simulation phase of our method, generating simulated anomalous time series windows (Definition 3.8).

Each state transition recorded in the event log contributes to building the control-flow structure, which is different for the two types of anomalies. A clear difference is the looping of the $3 \rightarrow 0$ and $0 \rightarrow 3$ state transitions. This is consistent with the sample velocity time series windows at the top, in which, after a negligible alternation of state transitions of little duration, these two state transitions appear repeatedly. While the weight anomaly also has this looping, it only appears at the start, which then follows with the main loop, which involves the $4 \rightarrow 1$ and $1 \rightarrow 4$ state transitions. This can be observed from the weight time series windows at the bottom. There are also state transitions that only appear exclusively in either the velocity or weight Petri net, such as the $4 \rightarrow 3$ state transition. It is worth noting that the Petri nets are influenced by the rapid state transitions that appear at the start of the time series window, which suggests that these should be discarded prior to their

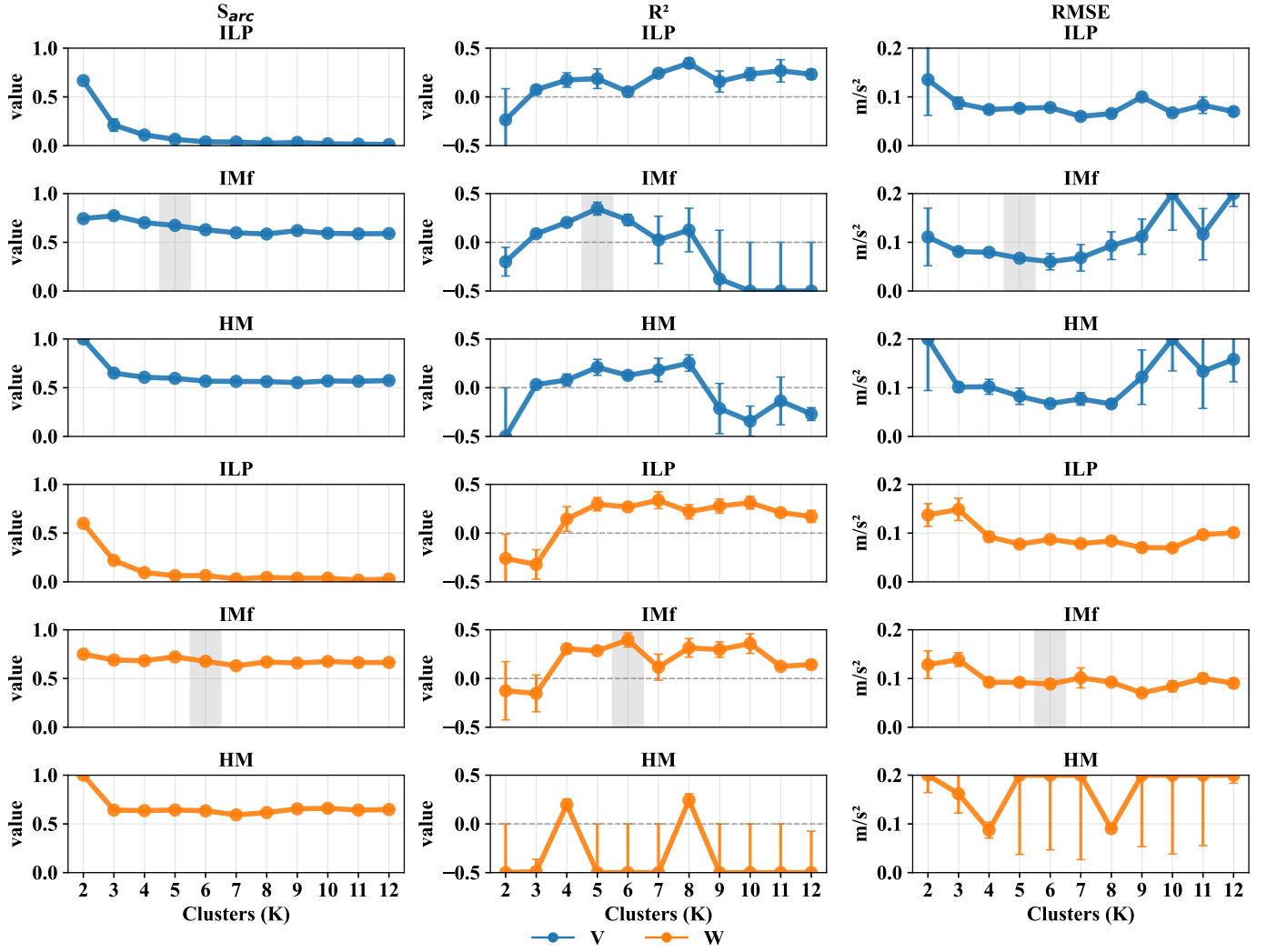


Figure 6: The S_{arc} , R^2 and RMSE trends for each process discovery algorithm with an increasing number of clusters K, for both the velocity (V) and weight (W) anomalies. The grey regions indicate the Petri nets achieving the best trade-off according to the three metrics.

generation.

The time perspective obtained by the state time distributions of the velocity and weight time series windows also reveals insightful information about the root causes of each anomaly. For example, the state time distribution heatmap of the weight anomaly reveals that some state times associated with specific state transitions can last for a long time with a fairly high probability, such as the $4 \rightarrow 1$ state transition, whose duration can be up to the 8-10 second interval with 19.4% probability. On the other hand, the time perspective of the velocity anomaly Petri net reveals that there are more state transitions occurring with shorter durations, while some state transitions are lengthier (within the 2-4 second range) with higher probabilities.

4.3. Fault identification

To assess the impact of clustering and process discovery configurations on the ability of our method to correctly distinguish faults from one another, we outline a two-factor full factorial

experiment, where the first factor is K, and the second factor is the process discovery algorithm. Table 4 reports the method results for the F1 and conformance checking time metrics. The N/A values indicate that conformance checking could not be performed due to the Petri net being non-sound or because the computation exceeded the total time limit of 300 seconds. Additionally, Figure 8 provides an interpretation of the results according to the ratios achieved by the fitness and RMSE metrics between positives and negatives, which play a pivotal role in fault identification (see Algorithm 1).

4.3.1. Results

F1 impact. The classification ability of the Petri nets depends heavily on the number of clusters K. For example, considering the weight anomaly, the ILP, IMF, and HM have as low as 15.528%, 12.472%, and 0.000% F1 values. On the other hand, for higher K values, F1 rises, with the ILP achieving perfect performance with K=7 for both the velocity and weight

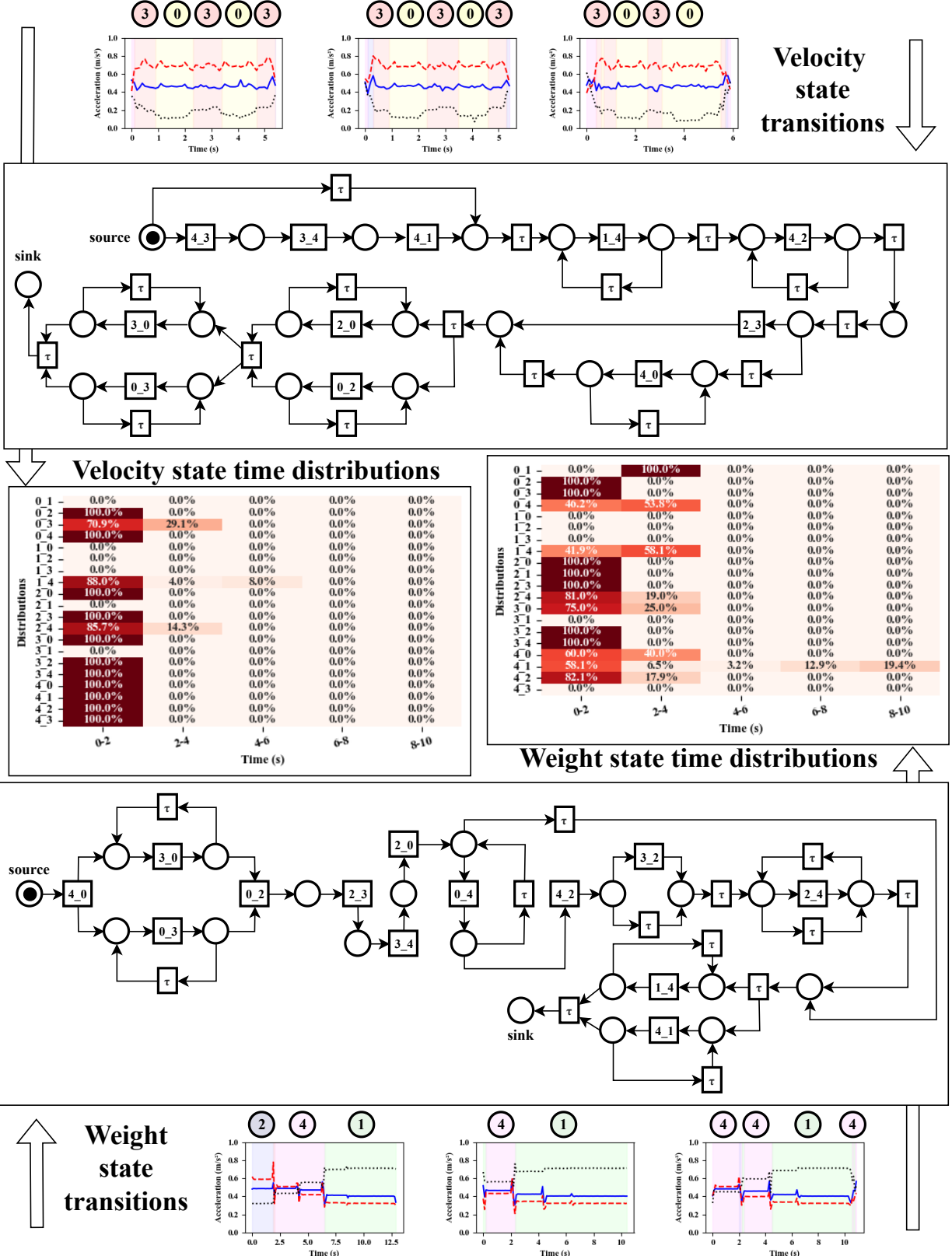


Figure 7: The control-flow structure and time perspective of the velocity and weight Petri nets generated through our method with the IMf and K=5.

Table 4: The fault identification results in terms of F1 score and conformance checking (CC) time of our fault diagnosis method for both the velocity and weight anomaly. $|P|+|Tr|$ indicates the total number of nodes in the Petri net extracted with the given process discovery algorithm–number of clusters combination, where $|P|$ and $|Tr|$ denote the cardinality of the sets of places and transitions, respectively. #E indicates the number of events in the event logs built with a given number of clusters. TE indicates that conformance checking exceeded the 300-second computation time, whereas NS indicates that the Petri net obtained with the process discovery algorithm-number of clusters combination is non-sound. The grey cells highlight the results of the best Petri nets identified in the modeling and simulation quality experiment. Bold numbers highlight the best F1 per process discovery algorithm and anomaly type.

ILP (75% noise tolerance)			IMF (75% noise tolerance)			HM (75% noise tolerance)			#E	
K	F1 (%)	CC time (s)	P + Tr	F1 (%)	CC time (s)	P + Tr	F1 (%)	CC time (s)	P + Tr	
Velocity anomaly	2	32.937 _{27.222}	0.004 _{0.000}	8 ₀	20.392 _{17.306}	0.004 _{0.000}	15 ₃	65.627 _{13.064}	0.003 _{0.000}	4 ₀ 67 ₄
	3	60.103 _{13.602}	0.006 _{0.000}	15 ₃	77.520 _{4.769}	0.007 _{0.000}	22 ₃	62.553 _{17.117}	0.007 _{0.000}	25 ₁ 156 ₁₅
	4	99.471 _{0.748}	0.011 _{0.000}	22 ₂	98.925 _{1.521}	0.010 _{0.000}	39 ₆	86.734 _{12.324}	0.008 _{0.001}	44 ₁ 209 ₃₀
	5	96.736 _{2.723}	0.026 _{0.003}	36 ₉	93.504 _{7.093}	0.020 _{0.002}	61 ₇	79.976 _{2.783}	0.015 _{0.004}	68 ₃ 300 ₁₀
	6	97.980 _{2.857}	0.061 _{0.019}	60 ₁₂	97.072 _{3.117}	0.158 _{0.091}	80 ₉	99.206 _{0.794}	0.029 _{0.013}	102 ₃ 480 ₁₈
	7	100.000 _{0.000}	0.129 _{0.058}	58 ₁₀	81.400 _{12.258}	1.478 _{1.369}	81 ₁₃	92.649 _{4.125}	0.029 _{0.001}	118 ₁ 537 ₁₂
	8	99.487 _{0.725}	0.177 _{0.086}	80 ₁₅	73.462 _{22.963}	2.303 _{1.553}	97 ₈	91.429 _{0.000}	0.054 _{0.000}	146 ₂ 563 ₁₆
	9	100.000 _{0.000}	0.145 _{0.032}	107 ₁	70.720 _{34.408}	1.205 _{0.966}	111 ₃	NS	NS	187 ₈ 614 ₁₄
	10	100.000 _{0.000}	0.239 _{0.030}	125 ₆	21.622 _{0.000}	8.899 _{0.000}	180 ₂₀	NS	NS	188 ₈ 733 ₁₀
	11	100.000 _{0.000}	0.507 _{0.215}	131 ₂₄	81.871 _{11.311}	64.984 _{53.965}	178 ₃₃	NS	NS	180 ₁₂ 763 ₁₇
	12	100.000 _{0.000}	1.491 _{1.501}	156 ₃	TE	TE	246 ₂₄	NS	NS	206 ₁₈ 763 ₂₅
Weight anomaly	2	15.528 _{8.305}	0.004 _{0.000}	9 ₀	12.472 _{14.845}	0.005 _{0.000}	12 ₀	0.000 _{0.000}	0.003 _{0.000}	4 ₀ 48 ₃
	3	61.187 _{9.589}	0.007 _{0.000}	15 ₁	73.447 _{3.501}	0.007 _{0.000}	21 ₁	49.313 _{9.275}	0.006 _{0.000}	29 ₁ 68 ₆
	4	98.990 _{1.429}	0.013 _{0.002}	23 ₁	98.039 _{2.773}	0.015 _{0.005}	31 ₄	82.185 _{9.047}	0.013 _{0.003}	38 ₄ 118 ₁₅
	5	94.213 _{4.548}	0.027 _{0.007}	30 ₂	90.600 _{9.234}	0.032 _{0.003}	43 ₄	70.175 _{3.509}	0.017 _{0.006}	43 ₁₁ 114 ₁₉
	6	95.556 _{6.285}	0.045 _{0.016}	30 ₁	91.232 _{10.204}	0.061 _{0.032}	60 ₉	98.485 _{1.515}	0.037 _{0.021}	43 ₁₄ 139 ₃₇
	7	100.000 _{0.000}	0.037 _{0.006}	61 ₇	74.100 _{13.199}	0.119 _{0.063}	103 ₈	87.059 _{7.059}	0.018 _{0.001}	58 ₆ 119 ₃
	8	98.925 _{1.521}	1.731 _{2.255}	48 ₁	70.381 _{21.026}	0.309 _{0.056}	114 ₂₂	76.923 _{0.000}	0.105 _{0.000}	57 ₆ 148 ₁₅
	9	100.000 _{0.000}	0.096 _{0.026}	56 ₃	78.930 _{18.599}	0.625 _{0.393}	123 ₁₆	NS	NS	60 ₁₀ 180 ₂₈
	10	100.000 _{0.000}	0.160 _{0.032}	60 ₃	50.848 _{0.000}	16.307 _{0.000}	119 ₂₇	NS	NS	41 ₇ 158 ₄₄
	11	100.000 _{0.000}	1.309 _{1.639}	92 ₆	65.662 _{24.284}	0.519 _{0.451}	123 ₂₂	NS	NS	83 ₄ 160 ₃₈
	12	100.000 _{0.000}	0.262 _{0.051}	136 ₂₅	TE	TE	192 ₆₁	NS	NS	72 ₁₂ 202 ₁₄

anomalies. Similarly, considering the velocity anomaly, the IMF and HM achieve F1 scores of 98.925% and 96.630% for K=4 and K=8, respectively. However, while the ILP maintains perfect classification for K \geq 7, the IMF and HM performance drop, which can be attributed to the results shown in the previous experiment. Notably, the ILP is unable to classify any trace for K=8, 9, and 10. This is due to the Petri net being non-sound, which makes it unsuitable for performing conformance checking. On the other hand, the IMF always produces sound Petri nets, so this process discovery algorithm is safe in this regard. These results are backed up by the visual interpretation provided in Figure 8, which shows that with increasing numbers of clusters, the ratios between positives and negatives of two out of the three metrics used during fault identification get higher than 1, meaning that there is a clear distinction between the anomalous velocity and weight time series windows.

Time impact. The conformance checking time tends to increase for each algorithm as the state complexity (K) of the Petri net increases. This trend is especially visible in the IMF, which achieves velocities and weights anomalies as low as 0.003 and 0.004 seconds at K=2, and peaks at 2.363 and 0.691 seconds at K=8 and 9, respectively. It finally exceeds the set time limit for K=10, 11, and 12. This is due to both the size of the Petri net in terms of the number of places and arcs, and the number of events of the event logs to check. In fact, the total number of places and transitions ($|P|+|Tr|$) of the Petri nets and the number of events (#E) increase significantly as the number of

clusters increases, leading to increasing conformance checking time too, as shown in Figure 8. Such behavior is to be expected, as conformance checking time tends to worsen as the number of events and structural complexity of the Petri net increase [12]. At times, the behavior of the conformance checking time is quite erratic. In fact, regarding the differences across various process discovery algorithms, the IMF shows some unexpected peaks, such as 16.307 seconds for the weight anomaly at K=10. It appears that ILP and HM are more stable, although the former has very low simplicity, whereas the latter may discover non-sound (NS) Petri nets.

4.3.2. Ablation test and comparisons

To further test the F1 performance of our method, we compared our method with other deep learning-based approaches (GRU-AE [57], LSTM-AE [58], and BiLSTM-AE [59]) with decreasing percentages of Acc (from 100% to 10%, see Equation 7) to evaluate the impact of this phase on the subsequent results. The chosen deep learning-based approaches can be adapted to the one-class classification setting of this study, where the training set only contains the sample of the target anomaly. For the comparison, we have used the IMF with K=5.

The F1 results are shown in Table 5. In the scenario where anomaly detection is flawless (Acc=100%), our method outperforms the other one-class approaches. However, as Acc values decrease, the other methods tend to perform better, although all of them drop to very low percentages when Acc reaches low values. This is to be expected: when the training set for fault

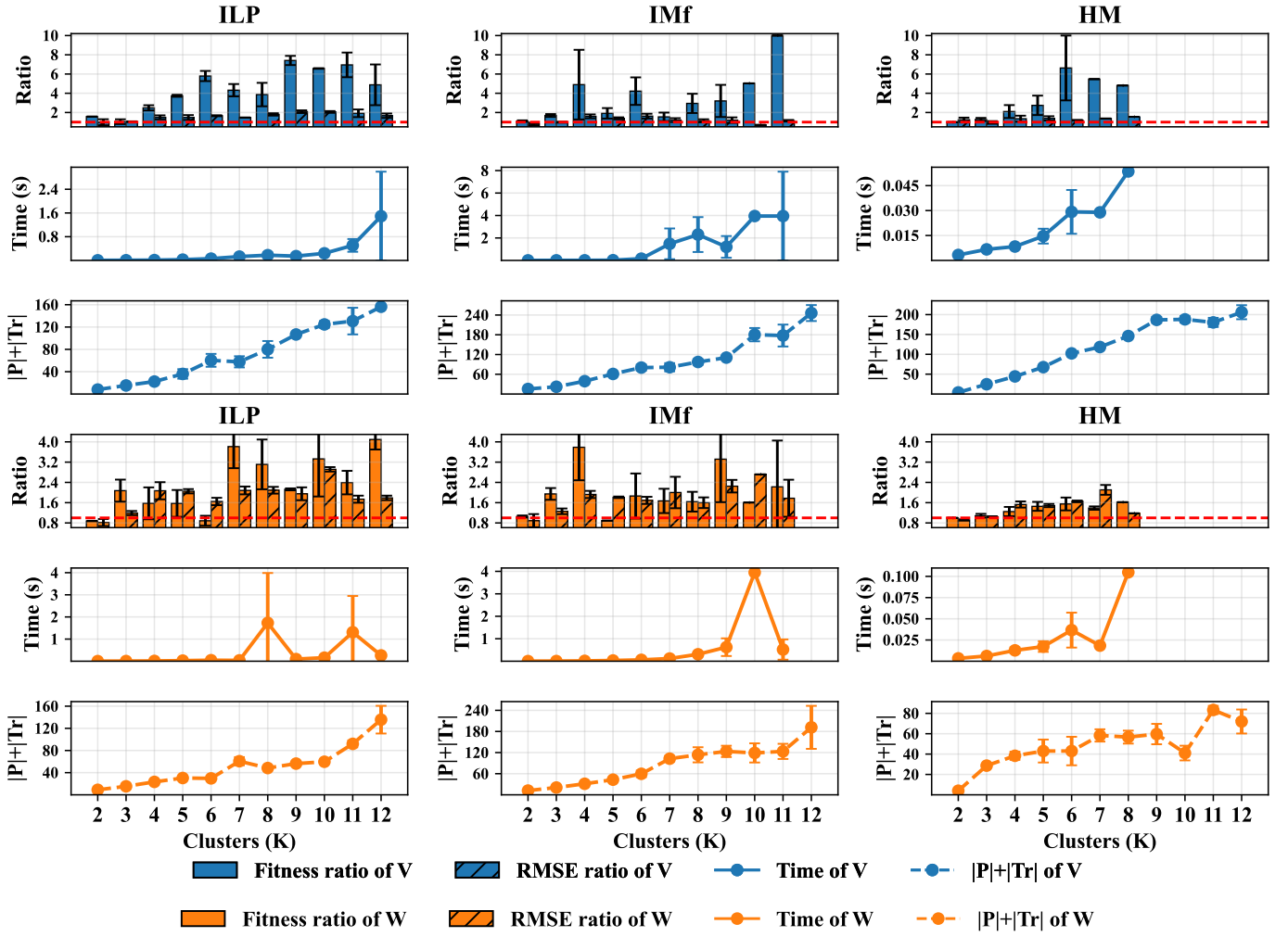


Figure 8: The fitness and RMSE ratio for each process discovery algorithm with an increasing number of clusters K, for both the velocity (V) and weight (W) anomalies. Below each ratio is the conformance checking time and the structural complexity of the Petri nets in terms of the number of places and transitions ($|P|+|Tr|$).

diagnosis is contaminated with normal time series windows, all the models are unable to properly characterize the specific fault, leading to worse performance. It is important to note that our method using the IMF with $K=5$ is less robust to contamination in normal behavior. This behavior can be explained using Figure 9. Higher accuracy (Acc) leads to higher fitness ratios between positives and negatives, which in turn results in better fault identification. As the accuracy decreases, the fitness ratio also declines, along with the quality of fault identification. This effect is much more pronounced for our proposed method than for the deep learning approaches. While this may be partly due to the sub-optimal choice of the IMF with $K=5$, it may also indicate that deep learning approaches are inherently more robust to noise [60]. However, the interpretation of deep learning methods is less straightforward because of their black-box nature.

4.4. Discussion

Modeling and simulation quality. In this part of the experimentation, we evaluated whether the methodology allowed the extraction of interpretable and accurate Petri nets. The experiments outlined that increasing the K factor led to slightly lower Petri net interpretability yet more accurate simulations in terms of R^2 and RMSE. However, this increase stops when the state space becomes too complex, causing the R^2 and RMSE to rise. Notably, while the ILP seems the most stable process discovery algorithm in terms of simulation accuracy, its arc-degree simplicity (S_{arc}) drops drastically, making the Petri nets unreadable. On the other hand, the IMF is the most balanced algorithm, achieving good interpretability and surpassing the HM in simulation accuracy. In conclusion, the different process discovery algorithms significantly impact the interpretability of Petri nets, while a trade-off for state complexity must be found regardless of the algorithm used.

	Acc	Ours	LSTM-AE	BiLSTM-AE	GRU-AE
Velocity anomaly	100%	98.430 _{0.020}	89.700 _{7.830}	94.550 _{1.570}	92.810 _{2.110}
	90%	82.170 _{4.570}	87.230 _{6.130}	87.120 _{3.680}	86.290 _{0.750}
	80%	84.580 _{2.420}	82.160 _{3.610}	82.630 _{1.700}	83.210 _{6.220}
	70%	57.710 _{14.210}	82.810 _{3.320}	84.120 _{4.390}	82.490 _{3.010}
	60%	39.750 _{6.600}	81.540 _{4.150}	83.610 _{6.500}	79.950 _{1.560}
	50%	48.380 _{12.160}	74.210 _{6.900}	77.430 _{6.670}	79.350 _{7.850}
	40%	41.940 _{22.020}	64.140 _{11.480}	67.060 _{19.770}	61.220 _{14.050}
	30%	25.560 _{9.890}	58.400 _{2.300}	70.130 _{6.550}	66.230 _{13.920}
	20%	24.540 _{15.810}	48.660 _{5.630}	40.870 _{5.190}	58.950 _{22.850}
	10%	11.700 _{9.750}	20.570 _{11.060}	16.880 _{4.270}	37.210 _{19.840}
Weight anomaly	100%	96.900 _{0.090}	84.150 _{3.360}	84.270 _{8.980}	83.170 _{11.670}
	90%	58.150 _{15.530}	75.540 _{4.890}	77.510 _{5.700}	67.810 _{3.630}
	80%	60.680 _{17.170}	64.020 _{1.050}	61.470 _{0.870}	57.950 _{2.660}
	70%	39.930 _{18.960}	61.960 _{1.120}	54.430 _{7.190}	48.140 _{3.340}
	60%	45.580 _{9.300}	58.340 _{4.380}	50.000 _{6.630}	41.380 _{6.940}
	50%	36.240 _{26.770}	54.910 _{4.030}	51.080 _{0.370}	46.740 _{5.790}
	40%	45.160 _{16.340}	53.800 _{2.400}	45.620 _{1.760}	46.850 _{6.790}
	30%	12.000 _{16.970}	50.830 _{0.030}	41.190 _{4.380}	38.280 _{10.510}
	20%	25.770 _{17.920}	49.800 _{5.280}	43.440 _{6.420}	34.930 _{11.340}
	10%	14.440 _{20.430}	20.570 _{11.060}	16.880 _{4.270}	37.210 _{19.840}

Table 5: Fault identification comparison between our method and other deep learning-based approaches with decreasing anomaly detection accuracy (Acc) percentages. Bold figures indicate the best F1 per Acc percentage.

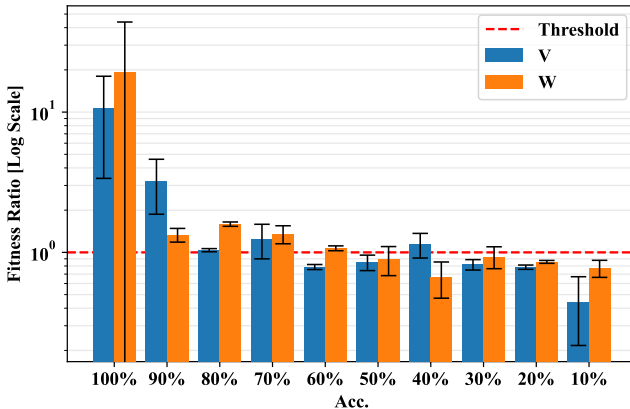


Figure 9: The fitness ratios for both the velocity (V) and weight (W) anomalies achieved by the IMf with K=5 per Acc percentage.

Fault Identification. Next, we evaluated whether the method enabled distinguishing between the two different anomaly types using the proposed fault identification algorithm. The K factor highly influences the F1-score results of our method, as low K values lead to poor classification results for all the process discovery algorithms and in both anomaly types. High K values may lead to higher F1-score, although it has been observed that this trend is not met by the IMf, whose performance tends to drop as K increases. Yet, while the ILP meets this trend, the algorithm may build non-sound Petri nets, which hinders the ability to perform alignment-based conformance checking. Regarding the time needed, conformance checking becomes more computationally expensive as K increases. Such an increase is due to both the heightened number of places and arcs of the Petri nets and the number of events resulting from the in-

creasing state space complexity. Finally, the ablation test and comparison highlighted that the accuracy of anomaly detection prior to fault identification has a significant impact on the F1 performance across our method and other deep learning-based approaches.

4.5. Threats to validity

The threats to validity regard possible construct, internal, and external pitfalls in the experimentation.

Construct validity. The experiments evaluated our method based on three aspects: Petri net interpretability, simulation accuracy, and fault diagnosis effectiveness. Petri net interpretability was measured via arc-degree simplicity, which provides information about structural properties but does not capture other control-flow aspects, such as cyclomatic complexity [61]. Simulation accuracy was assessed using RMSE and R², which reflect the similarity in amplitude and the variance explained by the simulated data, respectively. Other metrics, such as the Pearson correlation coefficient [62], could reveal additional aspects of simulation quality. Fault diagnosis effectiveness was evaluated using the F1-score, a standard classification metric; however, alternative metrics, such as the Matthews correlation coefficient [63], may provide complementary insights. Overall, while these metrics provide a valid and interpretable approximation of the aspects of interest, they may not fully capture all dimensions of process behavior.

Internal validity. We observed correlations between the state space complexity of the Petri net and the chosen process discovery algorithms on the modeling and simulation quality metrics, as shown in Table 3 and Figure 6. Similarly, these two factors have been shown to have a significant impact on fault identification capabilities, as illustrated in Table 4 and Figure 8. Finally, we have also evaluated the impact of anomaly detection accuracy on fault identification, and compared the results to other state-of-the-art methods for time series classification, as shown in Table 5. However, other factors may also have influenced these metrics. For example, the noisy nature of low-level sensor data can significantly impact the quality of the Petri nets. While we partially addressed this by setting a high noise threshold for all the algorithms, this challenge requires a more in-depth study.

External validity. Our study focused on the RoAD case study, which involved real multivariate time series data collected from various sensors mounted on a Kuka LBR iiwa robotic arm. While this dataset provides a solid foundation for evaluation, applying our methodology to additional CPSs would further strengthen the generalizability of our findings. Future studies could validate these results across different CPS environments to assess their broader applicability. Additionally, other faulty scenarios where regular trends do not follow each other as shown in Figure 5 should be studied to validate our approach to other manufacturing contexts.

5. Conclusions

The ever-increasing complexity of CPSs in production environments heightens the possibility of introducing vulnerabilities in their development and the occurrence of run-time faults. Therefore, reliable operation hinges on techniques that support interpretable and autonomous fault diagnosis capable of identifying deviations from normal behavior, classifying faults, and enhancing root-cause analysis. Yet, existing deep learning-based approaches yield black-box diagnoses that lack interpretability and the ability to understand the root causes of the occurred fault. On the other hand, Petri net-based approaches, valued for their clear, process-based semantics, either require manual, error-prone modeling by domain experts or do not directly target data-driven modeling of faulty CPS behaviors from low-level sensor data.

This study has demonstrated that process mining, specifically the discovery of interpretable Petri nets enriched with stochastic timing information, offers a principled, data-driven alternative that can help address the outlined challenges. To this aim, we introduced a process mining-driven fault diagnosis method that isolates anomalous sensor windows, converts them into event logs, and automatically derives stochastic Petri nets capable of replicating and explaining faulty dynamics. Extensive experiments have been performed on the Robotic Arm Dataset (RoAD), a benchmark collected from a robotic arm deployed in a scale-replica smart manufacturing assembly line. Results outline that the Petri nets obtained through our method (i) are able to strike a balance between interpretability and simulation accuracy, (ii) identify different types of faulty reliably with low classification times. Collectively, these findings confirm the viability of the obtained Petri nets as transparent, executable knowledge sources for CPS dependability analyses.

Future research will focus on enhancing manufacturing system reliability by applying the proposed method across various industrial settings, including advanced manufacturing lines and supply chain networks. Integrating the discovered fault models with predictive maintenance and smart scheduling platforms can drive early fault identification, reduce unplanned downtime, and optimize resource allocation on the factory floor. Additionally, coupling simulation-based fault diagnosis with safety assurance tools, such as digital twins and runtime monitoring, can offer manufacturers quantitative insights into system robustness, enabling more informed decisions to maintain continuous, safe, and efficient production operations under fault conditions.

Declaration of competing interest

The authors declare that they have no known competing financial interests or personal relationships that could have appeared to influence the work reported in this paper.

Acknowledgments

This study is supported by the Spoke 9 “Digital Society & Smart Cities” of ICSC - Centro Nazionale di Ricerca in High

Performance-Computing, Big Data and Quantum Computing, funded by the European Union - NextGenerationEU (PNRR-HPC, CUP: E63C22000980007), by the European Union’s Horizon Europe research and innovation programme under the Marie Skłodowska-Curie grant agreement No. 101109243, and by the Veneto Region within the PR Veneto FESR 2021-2027 program, Action 1.1.1 Sub A “Rafforzare la ricerca e l’innovazione tra imprese e organismi di ricerca” (DGR n. 729/2024), project “SUPREME” (CUP D19J24000680007 – ID 24729_001692). This manuscript reflects only the Authors’ views and opinions, neither the European Union nor the European Commission can be considered responsible for them.

Data availability

The code and dataset for this paper are available in the following GitHub repository: https://github.com/francescovitale/pm_based_modeling_simulation.

References

- [1] G. Wan, X. Dong, Q. Dong, Y. He, P. Zeng, Context-aware scheduling and control architecture for cyber-physical production systems, *Journal of Manufacturing Systems* 62 (2022) 550–560. [doi:
https://doi.org/10.1016/j.jmsy.2022.01.008](https://doi.org/10.1016/j.jmsy.2022.01.008).
- [2] J. Friederich, S. Lazarova-Molnar, Reliability assessment of manufacturing systems: A comprehensive overview, challenges and opportunities, *Journal of Manufacturing Systems* 72 (2024) 38–58. [doi:
https://doi.org/10.1016/j.jmsy.2023.11.001](https://doi.org/10.1016/j.jmsy.2023.11.001).
- [3] S. Li, B. Zhou, J. Shang, X. Chen, J. Yu, Review of recent applications and future perspectives on process monitoring approaches in industrial processes, *Journal of Manufacturing Systems* 82 (2025) 509–530. [doi:
https://doi.org/10.1016/j.jmsy.2025.07.002](https://doi.org/10.1016/j.jmsy.2025.07.002).
- [4] B. Gueuziec, J. Gallois, F. Boulanger, Qualitative Tendencies for Hybrid System Simulation, in: 2023 ACM/IEEE International Conference on Model Driven Engineering Languages and Systems Companion (MODELS-C), 2023, pp. 500–509. [doi:
https://doi.org/10.1109/MODELS-C59198.2023.00087](https://doi.org/10.1109/MODELS-C59198.2023.00087).
- [5] N. Tampouratzis, P. Mousouliotis, I. Papaefstathiou, A Novel Integrated Simulation Framework for Cyber-Physical Systems Modelling, *IEEE Transactions on Parallel and Distributed Systems* 34 (10) (2023) 2684–2698. [doi:
https://doi.org/10.1109/TPDS.2023.3300081](https://doi.org/10.1109/TPDS.2023.3300081).
- [6] A. Avizienis, J.-C. Laprie, B. Randell, C. Landwehr, Basic concepts and taxonomy of dependable and secure computing, *IEEE Transactions on Dependable and Secure Computing* 1 (2004) 11–33. [doi:
https://doi.org/10.1109/TDSC.2004.2](https://doi.org/10.1109/TDSC.2004.2).

[7] B. Cai, L. Huang, M. Xie, Bayesian Networks in Fault Diagnosis, *IEEE Transactions on Industrial Informatics* 13 (2017) 2227–2240. [doi:](https://doi.org/10.1109/TII.2017.2695583).

[8] W. Yu, C. Zhao, Broad Convolutional Neural Network Based Industrial Process Fault Diagnosis With Incremental Learning Capability, *IEEE Transactions on Industrial Electronics* 67 (6) (2020) 5081–5091. [doi:](https://doi.org/10.1109/TIE.2019.2931255).

[9] C. Li, S. Li, H. Wang, F. Gu, A. D. Ball, Attention-based deep meta-transfer learning for few-shot fine-grained fault diagnosis, *Knowledge-Based Systems* 264 (2023) 110345. [doi:](https://doi.org/10.1016/j.knosys.2023.110345).

[10] M. A. Belay, A. Rasheed, P. S. Rossi, MTAD: Multiobjective Transformer Network for Unsupervised Multisensor Anomaly Detection, *IEEE Sensors Journal* 24 (12) (2024) 20254–20265. [doi:](https://doi.org/10.1109/JSEN.2024.3396690).

[11] K. M. Hanga, Y. Kovalchuk, M. M. Gaber, A Graph-Based Approach to Interpreting Recurrent Neural Networks in Process Mining, *IEEE Access* 8 (2020) 172923–172938. [doi:](https://doi.org/10.1109/ACCESS.2020.3025999).

[12] W. M. P. van der Aalst, J. Carmona, *Process Mining Handbook*, Springer, Cham, Switzerland, 2022. [doi:](https://doi.org/10.1007/978-3-031-08848-3).

[13] H. Liu, Y. Wang, W. Fan, X. Liu, Y. Li, S. Jain, Y. Liu, A. Jain, J. Tang, Trustworthy AI: A Computational Perspective, *ACM Transactions on Intelligent Systems and Technology* 14 (1) (2022) 1–59. [doi:](https://doi.org/10.1145/3546872).

[14] A. S. Mozafari Mehr, R. M. de Carvalho, B. van Dongen, Explainable conformance checking: Understanding patterns of anomalous behavior, *Engineering Applications of Artificial Intelligence* 126 (2023) 106827. [doi:](https://doi.org/10.1016/j.engappai.2023.106827).

[15] S. Hu, Z. Li, R. Wisniewski, Optimal Sensor Selection for Diagnosability Enforcement in Labeled Petri Nets, *IEEE Transactions on Systems, Man, and Cybernetics: Systems* 54 (2024) 2965–2977. [doi:](https://doi.org/10.1109/TSMC.2024.3351740).

[16] M. Mansour, M. A. Wahab, W. M. Soliman, Petri nets for fault diagnosis of large power generation station, *Ain Shams Engineering Journal* 4 (4) (2013) 831–842. [doi:](https://doi.org/10.1016/j.asej.2013.04.006).

[17] S. Liu, X. Hu, J. Wang, Hierarchical Modeling Fault-Error-Failure Dependencies for Cyber-Physical Systems, in: *Proceedings of The Eighth International Conference on Bio-Inspired Computing: Theories and Applications* (BIC-TA), 2013, 2013, pp. 641–649. [doi:](https://doi.org/10.1007/978-3-642-37502-6_77).

[18] P. Nazemzadeh, A. Dideban, M. Zareiee, Fault Modeling in Discrete Event Systems Using Petri Nets, *ACM Transactions on Embedded Computing Systems* 12. [doi:](https://doi.org/10.1145/2406336.2406348).

[19] M. Bourdeau, X. qiang Zhai, E. Nefzaoui, X. Guo, P. Chatellier, Modeling and forecasting building energy consumption: A review of data-driven techniques, *Sustainable Cities and Society* 48 (2019) 101533. [doi:](https://doi.org/10.1016/j.scs.2019.101533).

[20] F. Vitale, F. De Vita, N. Mazzocca, D. Bruneo, A Process Mining-based unsupervised Anomaly Detection technique for the Industrial Internet of Things, *Internet of Things* 24 (2023) 100993. [doi:](https://doi.org/10.1016/j.iot.2023.100993).

[21] H. H. Beyel, O. Makke, M. Pourbafrani, O. Gusikhin, W. M. P. van der Aalst, Analyzing Data Streams from Cyber-Physical-Systems: A Case Study, *SN Computer Science* 5 (2024) 1–17. [doi:](https://doi.org/10.1007/s42979-024-03008-8).

[22] F. Vitale, S. Guarino, F. Flammini, L. Faramondi, N. Mazzocca, R. Setola, Process Mining for Digital Twin Development of Industrial Cyber-Physical Systems, *IEEE Transactions on Industrial Informatics* 21 (1) (2025) 866–875. [doi:](https://doi.org/10.1109/TII.2024.3465600).

[23] A. C. da Silveira, Álvaro Sobrinho, L. Dias da Silva, D. F. Santos, M. Nauman, A. Perkusich, Harnessing coloured Petri nets to enhance machine learning: A simulation-based method for healthcare and beyond, *Simulation Modelling Practice and Theory* 140 (2025) 103080. [doi:](https://doi.org/10.1016/j.simpat.2025.103080).

[24] S. Lassoued, A. Schwung, Introducing PetriRL: An innovative framework for JSSP resolution integrating Petri nets and event-based reinforcement learning, *Journal of Manufacturing Systems* 74 (2024) 690–702. [doi:](https://doi.org/10.1016/j.jmsy.2024.04.028).

[25] K. Nadim, A. Ragab, M.-S. Ouali, Data-driven dynamic causality analysis of industrial systems using interpretable machine learning and process mining, *Journal of Intelligent Manufacturing* 34 (1) (2022) 57–83. [doi:](https://doi.org/10.1007/s10845-021-01903-y).

[26] F. Wittbold, R. Bernemann, R. Heckel, T. Heindel, B. König, Stochastic Decision Petri Nets, in: *Application and Theory of Petri Nets and Concurrency*, 2023, pp. 264–285. [doi:](https://doi.org/10.1007/978-3-031-33620-1_15).

[27] A. Rogge-Solti, W. M. P. van der Aalst, M. Weske, Discovering Stochastic Petri Nets with Arbitrary Delay Distributions from Event Logs, in: Business Process Management Workshops, 2014, pp. 15–27. [doi:
https://doi.org/10.1007/978-3-319-06257-0_2](https://doi.org/10.1007/978-3-319-06257-0_2).

[28] M. Cabasino, A. Giua, M. Poccia, C. Seatzu, Discrete event diagnosis using labeled Petri nets. An application to manufacturing systems, *Control Engineering Practice* 19 (90) (2011) 989–1001. [doi:
https://doi.org/10.1016/j.conengprac.2010.12.010](https://doi.org/10.1016/j.conengprac.2010.12.010).

[29] A. C. Bonafin, F. G. Cabral, M. V. Moreira, An effective approach for fault diagnosis of Discrete-Event Systems modeled as safe labeled Petri nets, *Control Engineering Practice* 123 (2022) 105168. [doi:
https://doi.org/10.1016/j.conengprac.2022.105168](https://doi.org/10.1016/j.conengprac.2022.105168).

[30] J. Liu, E. S. B. Mvungi, X. Zhang, A. Dias, Fault Diagnosis in Partially Observable Petri Nets with Quantum Bayesian Learning, *Applied Sciences* 14 (2024) 1–52. [doi:
https://doi.org/10.3390/app14010052](https://doi.org/10.3390/app14010052).

[31] G. Zhu, Z. Li, N. Wu, A. Al-Ahmari, Fault Identification of Discrete Event Systems Modeled by Petri Nets With Unobservable Transitions, *IEEE Transactions on Systems, Man, and Cybernetics: Systems* 49 (2) (2019) 333–345. [doi:
https://doi.org/10.1109/TSMC.2017.2762823](https://doi.org/10.1109/TSMC.2017.2762823).

[32] W. Hou, J. Ye, J. Wang, Fault identification of DES using Petri net, in: 2021 IEEE International Conference on Networking, Sensing and Control (ICNSC), 2021, pp. 1–6. [doi:
https://doi.org/10.1109/ICNSC52481.2021.9702163](https://doi.org/10.1109/ICNSC52481.2021.9702163).

[33] A. Neshastegaran, A. Norouzifar, I. Izadi, A Framework for Plant Topology Extraction Using Process Mining and Alarm Data, in: 2022 30th International Conference on Electrical Engineering (ICEE), 2022, pp. 485–491. [doi:
https://doi.org/10.1109/ICEE55646.2022.9827266](https://doi.org/10.1109/ICEE55646.2022.9827266).

[34] J. Friederich, S. Lazarova-Molnar, Data-Driven Reliability Modeling of Smart Manufacturing Systems Using Process Mining, in: 2022 Winter Simulation Conference (WSC), 2022, pp. 2534–2545. [doi:
https://doi.org/10.1109/WSC57314.2022.10015301](https://doi.org/10.1109/WSC57314.2022.10015301).

[35] X. Wang, L. Yang, D. Li, L. Ma, Y. He, J. Xiao, J. Liu, Y. Yang, MADD: Multi-Scale Anomaly Detection, Diagnosis and Correction for Discrete Event Logs, in: Proceedings of the 38th Annual Computer Security Applications Conference, 2022, pp. 769–784. [doi:
https://doi.org/10.1145/3564625.3567972](https://doi.org/10.1145/3564625.3567972).

[36] Y. Shi, N. Zhang, X. Song, H. Li, Q. Zhu, Novel approach for industrial process anomaly detection based on process mining, *Journal of Process Control* 136 (2024) 103165. [doi:
https://doi.org/10.1016/j.jprocont.2024.103165](https://doi.org/10.1016/j.jprocont.2024.103165).

[37] A. De Benedictis, F. Flammini, N. Mazzocca, A. Somma, F. Vitale, Digital Twins for Anomaly Detection in the Industrial Internet of Things: Conceptual Architecture and Proof-of-Concept, *IEEE Transactions on Industrial Informatics* 19 (12) (2023) 11553–11563. [doi:
https://doi.org/10.1109/TII.2023.3246983](https://doi.org/10.1109/TII.2023.3246983).

[38] H. Feng, C. Gomes, S. Gil, P. H. Mikkelsen, D. Tola, P. G. Larsen, M. Sandberg, Integration Of The Mape-K Loop In Digital Twins, in: 2022 Annual Modeling and Simulation Conference (ANNSIM), 2022, pp. 102–113. [doi:
https://doi.org/10.23919/ANNSIM55834.2022.9859489](https://doi.org/10.23919/ANNSIM55834.2022.9859489).

[39] M. A. Farahani, M. McCormick, R. Gianinny, F. Hudecheck, R. Harik, Z. Liu, T. Wuest, Time-series pattern recognition in smart manufacturing systems: A literature review and ontology, *Journal of Manufacturing Systems* 69 (2023) 208–241. [doi:
https://doi.org/10.1016/j.jmsy.2023.05.025](https://doi.org/10.1016/j.jmsy.2023.05.025). URL <https://www.sciencedirect.com/science/article/pii/S0278612523000997>

[40] I. Elía, M. Pagola, Anomaly detection in smart-manufacturing era: A review, *Engineering Applications of Artificial Intelligence* 139 (2025) 109578. [doi:
https://doi.org/10.1016/j.engappai.2024.109578](https://doi.org/10.1016/j.engappai.2024.109578). URL <https://www.sciencedirect.com/science/article/pii/S0952197624017366>

[41] Z. Zamanzadeh Darban, G. I. Webb, S. Pan, C. Aggarwal, M. Salehi, Deep Learning for Time Series Anomaly Detection: A Survey, *ACM Computing Surveys* 57 (1) (2024) 1–42. [doi:
https://doi.org/10.1145/3691338](https://doi.org/10.1145/3691338).

[42] A. Chatterjee, B. S. Ahmed, IoT anomaly detection methods and applications: A survey, *Internet of Things* 19 (2022) 100568. [doi:
https://doi.org/10.1016/j.iot.2022.100568](https://doi.org/10.1016/j.iot.2022.100568).

[43] A. A. Cook, G. Misirli, Z. Fan, Anomaly Detection for IoT Time-Series Data: A Survey, *IEEE Internet of Things Journal* 7 (2020) 6481–6494. [doi:
https://doi.org/10.1109/JIOT.2019.2958185](https://doi.org/10.1109/JIOT.2019.2958185).

[44] V. Chandola, A. Banerjee, V. Kumar, Anomaly Detection for Discrete Sequences: A Survey, *IEEE Transactions on Knowledge and Data Engineering* 24 (5) (2012) 823–839. [doi:
https://doi.org/10.1109/TKDE.2010.235](https://doi.org/10.1109/TKDE.2010.235).

[45] H. Qin, X. Zhan, Y. Zheng, CSCAD: Correlation Structure-Based Collective Anomaly Detection in Complex System, *IEEE Transactions on Knowledge and Data Engineering* 35 (5) (2023) 4634–4645. [doi:
https://doi.org/10.1109/TKDE.2022.3154166](https://doi.org/10.1109/TKDE.2022.3154166).

[46] A. Hemmer, M. Abderrahim, R. Badonnel, J. François, I. Chrisment, Comparative Assessment of Process Mining for Supporting IoT Predictive Security, *IEEE Transactions*

on Network and Service Management 18 (1) (2021) 1092–1103. [doi:
https://doi.org/10.1109/TNSM.2020.3038172](https://doi.org/10.1109/TNSM.2020.3038172).

[47] Z. Su, T. Yu, A. Polyvyanyy, Y. Tan, N. Lipovetzky, S. Sardiña, N. van Beest, A. Mohammadi, D. Oetomo, Process mining over sensor data: Goal recognition for powered transhumeral prostheses, *Information Systems* 132 (2025) 102540. [doi:
https://doi.org/10.1016/j.is.2025.102540](https://doi.org/10.1016/j.is.2025.102540).

[48] M. L. van Eck, N. Sidorova, W. M. P. van der Aalst, Enabling process mining on sensor data from smart products, in: 2016 IEEE Tenth International Conference on Research Challenges in Information Science (RCIS), 2016, pp. 1–12. [doi:
https://doi.org/10.1109/RCIS.2016.7549355](https://doi.org/10.1109/RCIS.2016.7549355).

[49] S. J. J. Leemans, D. Fahland, W. M. P. van der Aalst, Discovering Block-Structured Process Models from Event Logs - A Constructive Approach, in: Application and Theory of Petri Nets and Concurrency, 2013, pp. 311–329. [doi:
https://doi.org/10.1007/978-3-642-38697-8_17](https://doi.org/10.1007/978-3-642-38697-8_17).

[50] S. J. van Zelst, B. F. van Dongen, W. M. van der Aalst, H. M. Verbeek, Discovering workflow nets using integer linear programming, *Computing* 100 (2018) 529–556. [doi:
https://doi.org/10.1007/s00607-017-0582-5](https://doi.org/10.1007/s00607-017-0582-5).

[51] A. Weijters, J. Ribeiro, Flexible heuristics miner (fhm), in: 2011 IEEE Symposium on Computational Intelligence and Data Mining (CIDM), 2011, pp. 310–317. [doi:
https://doi.org/10.1109/CIDM.2011.5949453](https://doi.org/10.1109/CIDM.2011.5949453).

[52] B. Vázquez-Barreiros, M. Mucientes, M. Lama, ProDiGen: Mining complete, precise and minimal structure process models with a genetic algorithm, *Information Sciences* 294 (2015) 315–333. [doi:
https://doi.org/10.1016/j.ins.2014.09.057](https://doi.org/10.1016/j.ins.2014.09.057).

[53] A. Mascolini, S. Gaiardelli, F. Ponzio, N. Dall’Ora, E. Macii, S. Vinco, S. Di Cataldo, F. Fummi, Robotic Arm Dataset (RoAD): A Dataset to Support the Design and Test of Machine Learning-Driven Anomaly Detection in a Production Line, in: IECON 2023- 49th Annual Conference of the IEEE Industrial Electronics Society, 2023, pp. 1–7. [doi:
https://doi.org/10.1109/IECON51785.2023.10311726](https://doi.org/10.1109/IECON51785.2023.10311726).

[54] V. Golendukhina, B. Wiesmayr, M. Felderer, A Review of Publicly Available Datasets from Manufacturing Systems, in: 2024 IEEE 29th International Conference on Emerging Technologies and Factory Automation (ETFA), 2024, pp. 1–8. [doi:
https://doi.org/10.1109/ETFA61755.2024.10710865](https://doi.org/10.1109/ETFA61755.2024.10710865).

[55] U. Khan, D. Cheng, F. Setti, F. Fummi, M. Cristani, L. Capogrosso, A Comprehensive Survey on Deep Learning-based Predictive Maintenance, *ACM Transactions on Embedded Computing Systems* [doi:
https://doi.org/10.1145/3732287](https://doi.org/10.1145/3732287).

[56] S. J. J. Leemans, D. Fahland, W. M. P. van der Aalst, Discovering Block-Structured Process Models from Event Logs Containing Infrequent Behaviour, in: Business Process Management Workshops, 2014, pp. 66–78. [doi:
https://doi.org/10.1007/978-3-319-06257-0_6](https://doi.org/10.1007/978-3-319-06257-0_6).

[57] Y. Guo, W. Liao, Q. Wang, L. Yu, T. Ji, P. Li, Multidimensional Time Series Anomaly Detection: A GRU-based Gaussian Mixture Variational Autoencoder Approach, in: Proceedings of The 10th Asian Conference on Machine Learning, 2018, pp. 97–112. URL <https://proceedings.mlr.press/v95/guo18a.html>

[58] P. Malhotra, A. Ramakrishnan, G. Anand, L. Vig, P. Agarwal, G. Shroff, LSTM-based encoder-decoder for multi-sensor anomaly detection (2016). [doi:
https://doi.org/10.48550/arXiv.1607.00148](https://doi.org/10.48550/arXiv.1607.00148).

[59] A. S. Raihan, I. Ahmed, A Bi-LSTM Autoencoder Framework for Anomaly Detection – A Case Study of a Wind Power Dataset (2023). [arXiv:2303.09703](https://arxiv.org/abs/2303.09703), doi: <https://doi.org/10.48550/arXiv.2303.09703>.

[60] J. Wang, Z. Wu, M. Lu, J. Ai, An empirical study on the effect of training data perturbations on neural network robustness, *Sensors* 24 (15) (2024) 4874. [doi:
https://doi.org/10.3390/s24154874](https://doi.org/10.3390/s24154874).

[61] K. B. Lassen, W. M. van der Aalst, Complexity metrics for Workflow nets, *Information and Software Technology* 51 (3) (2009) 610–626. [doi:
https://doi.org/10.1016/j.infsof.2008.08.005](https://doi.org/10.1016/j.infsof.2008.08.005).

[62] P. Schober, C. Boer, L. A. Schwarte, Correlation coefficients: appropriate use and interpretation, *Anesthesia & analgesia* 126 (5) (2018) 1763–1768.

[63] D. Chicco, N. Tötsch, G. Jurman, The Matthews correlation coefficient (MCC) is more reliable than balanced accuracy, bookmaker informedness, and markedness in two-class confusion matrix evaluation, *BioData mining* 14 (1) (2021) 13. [doi:
https://doi.org/10.1186/s13040-021-00244-z](https://doi.org/10.1186/s13040-021-00244-z).